Journal of Thermal Analysis and Calorimetry (2023) 148:1265–1287
https://doi.org/10.1007/s10973-022-11617-9

Sunset Yellow: physical, thermal and bioactive properties of the widely employed food, pharmaceutical and cosmetic orange azo-dye material

Marian Leulescu[1] · Ion Pălărie[1] · Andrei Rotaru[2,3,4] · Anca Moanţă[5] · Nicoleta Cioateră[5] · Mariana Popescu[6] · Gabriela Iacobescu[1] · Emilian Morîntale[1] · Mihaela Bojan[7] · Maria Ciocîlteu[6] · Iulian Petrişor[1] · Petre Rotaru[1]

Received: 10 October 2021 / Accepted: 11 September 2022 / Published online: 4 October 2022

Abstract

Sunset Yellow (E110) is an azoic dye synthetized from aromatic hydrocarbons, which is used to improve the physical–chemical properties of food products and their conservation; its chemical formula is $C_{16}H_{10}N_2Na_2O_7S_2$. Here, in order to characterize this azoic dye in powder and solution form, five spectral techniques were employed: Fourier Transform Infrared (FTIR), UV–Vis, Raman, Laser fluorescence and Terahertz (THz) spectroscopy. The Sunset Yellow's morphology, structure and its chemical composition were studied by scanning electron microscopy (SEM), X-ray diffraction and energy-dispersive X-ray spectroscopy (EDXS). The thermal behaviour of Sunset Yellow was studied in correlation with its physical (refractive index, electric susceptivity, optical anisotropy) and chemical (acidity) properties. Thermal analysis effectuated in air indicates the evaporation of absorbed and physically bonded water up to 188 °C, after which the material possesses thermal stability up to 330 °C. The oxidative decomposition takes place in four exothermic steps of which the strongest between 510 and 643 °C develops a heat of 4519.6 J g^{-1}; at 913 °C, a residue of 31.77% is obtained. The study of optical properties of Sunset Yellow shows that the refractive indexes are decreasing when the temperature of the solution increases. The optical anisotropy of Sunset Yellow was studied under polarized light at room temperature. Sunset Yellow exhibits the phenomenon of birefringence on resulted crystallites by drying and crystallization at RT from aqueous solutions with concentrations of 1% and 5%. THz spectroscopy identified the THz spectral "signature" of Sunset Yellow at a few wavelengths. Sunset Yellow has biophysical properties when interacting with proteins (bovine serum albumin (BSA) and collagen). The biological properties of Sunset Yellow were observed through its antioxidant activity and phytotoxicity; while the antioxidant activity is proportional with increasing its concentration, the phytotoxicity study indicates that the Sunset Yellow does not present wheat (Triticum aestivum) growth phytotoxicity at low concentrations (when treating with aqueous solutions of 0.01–0.05%, it could increase its resistance to drought conditions), but at concentrations of 0.25% or higher, there are negative changes in wheat growth.

Keywords Azo dye · Biophysical activity · Food and cosmetic colouring material · Orange and yellow-range azo dye · Physical properties · Sunset Yellow · Thermal stability

✉ Andrei Rotaru
andrei.rotaru@edu.ucv.ro; andrei.rotaru@icf.ro

[1] Department of Physics, Faculty of Sciences, University of Craiova, Str. A.I. Cuza Street, Nr. 13, 200585 Craiova, Romania

[2] Department of Biology and Environmental Engineering, Faculty of Horticulture, University of Craiova, Str. A.I. Cuza, Nr. 13, 200585 Craiova, Romania

[3] Department of Chemical Thermodynamics, Institute of Physical Chemistry "Ilie Murgulescu", Romanian Academy, Splaiul Independentei, Nr. 202, 060021 Bucharest, Romania

[4] Department of Chemistry, Faculty of Biology and Chemistry, "Ion Creangă" State Pedagogical University of Chișinău, Str. Drumul Viilor, Nr. 26A, Chişinău, Republic of Moldova

[5] Department of Chemistry, Faculty of Sciences, University of Craiova, Str. Calea Bucuresti, Nr. 107 I, 200478 Craiova, Romania

[6] Faculty of Pharmacy, University of Medicine and Pharmacy of Craiova, Str. Petru Rareş, Nr. 2, 200349 Craiova, Romania

[7] Laser Department, INFLPR –National Institute for Laser, Plasma and Radiation Physics, Bvd. Atomistilor, Nr. 409, PO Box MG-16, 077125 Măgurele (Ilfov), Bucharest, Romania

Introduction

Sunset Yellow is an orange-yellow powder azo-food dye with the chemical formula $C_{16}H_{10}N_2Na_2O_7S_2$ and with the molar mass of 452.37 g mol^{-1} [1]. It is a biologically active material, with limited absorption in the gastrointestinal tract, while the free sulphonated aromatic amines may reach the systemic circulation [1–3]. According to International Numbering System (INS), it has received the code 110 (E110 in Europe) [4], especially when used as a colouring agent of foods and pharmaceuticals [3], and the code CI 15,985 when used as a cosmetic ingredient [4]. Its full chemical name is disodium 2-hydroxy-1-(4-sulphonatophenylazo) naphthalene-6-sulphonate. Acceptable daily intake (ADI) of this dye is 4 mg/kg body weight/day [2].

Sunset Yellow is regulated by the Food and Agriculture Organization and World Health Organization (FAO/WHO), Joint FAO/WHO Expert Committee on Food Additives (JECFA) [5], EFSA (European Food Safety Authority) [1] and is defined by the European Commission (EC) Regulation 1333/2008 [6]. Its structural formula is presented in Fig. 1 [7].

Until now, the main method for the determination of Sunset Yellow in foods was the high-performance liquid chromatography (HPLC) [8, 9], while other techniques did not led to the elucidation of their physical–chemical properties [10]; however, many studies of on such azo dyes involving thermal analysis and calorimetry methods proved to be prodigious [11–36].

Here, many other properties of Sunset Yellow, such as the spectral, morphological, structural and compositional characteristics, are investigated. Also, the thermal behaviour of Sunset Yellow was studied in correlation with its physical (refractive index, electric susceptivity, optical anisotropy) and chemical (acidity) properties. Moreover, the biophysical properties (interaction with proteins) and biological activity (antioxidative and phytotoxicity properties) of Sunset Yellow were studied.

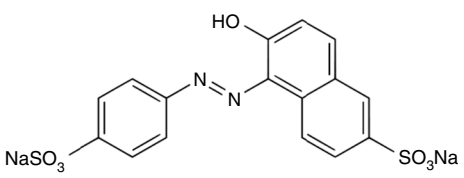

Fig. 1 Structural formula of Sunset Yellow

Experimental

Materials

Sunset Yellow was purchased from S.C. ORIETTA IMPEX S.R.L., the supplier guaranteeing a 100% content of powdered food dye. Sunset Yellow consists essentially of disodium 2-hydroxy-1-(4-sulphonatophenylazo) naphthalene-6-sulphonate and subsidiary colouring matters, together with sodium chloride and/or sodium sulphate as the principal uncoloured components. Sunset Yellow is described as the disodium salt. The calcium and the potassium salts are also permitted (Directive 2008/128/EC) [1, 6].

The purity is specified as not less than 85% total colouring matters, calculated as the disodium salt. The remaining 15% may be accounted for by sodium chloride or sodium sulphate, $\leq 5\%$ subsidiary colouring matters and $\leq 0.5\%$ 4-aminonaphthalene-1-sulphonic acid, 7-hydroxynaphthalene-1,3-disulphonic acid, 3-hydroxynaphthalene-2,7-disulphonic acid, 6-hydroxynaphthalene-2-sulphonic acid, 4,4′-diazoaminodi(benzene sulphonic acid) and 6,6′-oxydi(naphthalene-1,3-disulphonic acid), originating from the manufacturing process [1]. If the existing specifications could be extended to include $\leq 15.0\%$ sodium chloride and/or sodium sulphate as the principal uncoloured components, 99.9% of the material would be accounted for [1]. The specifications for Sunset Yellow according to Commission Directive 2008/128/EC and JECFA (JECFA, 2006) allowed the presence of up to 5% subsidiary colouring matters.

Used methods and techniques

The refractive index of the Sunset Yellow's solutions was obtained with the RA-520N refractometer which allows the samples to be heated on the temperature range 15–50 °C.

The measurement precision of the refractive index is ± 0.00002.

The Sunset Yellow's optical anisotropy was performed with the polarized light microscope LEICA DM 2500 P equipped with a video-recorder camera (Linkam Scientific Instruments Ltd.) at room temperature (RT) [13]. Sunset Yellow was examined between the cross-polarizers of the polarizing light microscope. The samples were exposed on COVN-024-200 (24×24 mm, 0.13–0.16 mm thick) COVER GLASS from Labbox and exhibits the phenomenon of birefringence obtained in resulted crystallites by the drying at RT of the Sunset Yellow's aqueous solutions with concentrations $c = 1\%$ and $c = 5\%$ [37, 38].

Infrared spectral measurements were performed with a Spectrum 100 PerkinElmer spectrometer which explores

the range of 4000–400 cm^{-1} wavenumbers with a precision of 0.50 cm^{-1}. For each spectrum, the average of 10 acquired spectra was performed. The Sunset Yellow's spectrum was obtained using universal attenuated total reflectance (UATR) accessory, at a resolution of 4 cm^{-1}, and CO_2/H_2O correction [12, 16, 21].

The Raman spectra were obtained with RENISHAW in Via Raman Microscope which monitors shifts in Raman band's positions (down to as low as 0.02 cm^{-1}), resolves spectral features narrower than 0.5 cm^{-1}, measures Raman bands down to below 10 cm^{-1} (0.3 THz), acquires spectra from Raman bands down to 5 cm^{-1} (0.15 THz).

UV–Vis measurements were performed with the Ocean Optics S2000 UV–Vis Spectrophotometer using the Ar^+ laser radiation with a wavelength of 476.5 nm [39].

Sunset Yellow's atomic fluorescence was obtained with the Ar^+ INOVA 308C laser from Coherent. Excitation radiation had the power of 440 mW and was measured with a Max Field Top 2 power meter from Coherent [40].

Sunset Yellow's THz spectrum was obtained with the experimental set-up of THz-TDS system (an Ekspla THz kit with a FemtoFiber laser produced by TOPTICA). The system can measure a transmission spectrum in the THz domain (0.2–4.5 THz), by measuring the signal detected synchronous with a lock-in amplifier. The samples were measured on the same type of holder, made from medium density (MD) polyethylene [41].

The Sunset Yellow's morphology and its chemical composition were studied with an scanning electron microscope (SU8010 from Hitachi) equipped with an energy-dispersive X-ray spectroscopy unit (EDXS) from Oxford Instruments, which used a beam energy of 15 keV. The scanning electron microscope (SEM) has registered the Sunset Yellow's images at an accelerating voltage of 2 kV and 8200–9800 nA intensity of the emission electric current, allowing for magnifications between 1000× and 5000× and a scale detail of 10–50 µm.

Thermal analysis measurements of Sunset Yellow were performed in air dynamic atmosphere (150 cm^3 min^{-1}), at 10 °C min^{-1} heating rate, up to 1000 °C using alumina crucibles, with PerkinElmer DIAMOND TG/DTA device.

The pH measurement of the Sunset Yellow's aqueous solution was carried out with a pH and Temperature Sensor PasPort, with Data Studio soft PS-2102, from Pasco Scientific, which can measure pH from 0 to 14 pH in a temperature range from −4 °C up to 80 °C, with the resolution of 0.01 pH, gel-filled Ag–AgCl electrode, maximum sample rate 50 Hz.

The biophysical properties of Sunset Yellow were analysed through its interaction with proteins from the bovine serum albumin (BSA) by UV–Vis spectroscopy and with the collagen by FTIR spectroscopy. The biological activity of Sunset Yellow was observed in its antioxidative and phytotoxicity activities.

Results and discussion

Refractive indices of Sunset Yellow (E110)

It can be observed that for both concentrations of 1% and 5%, refractive indices of aqueous Sunset Yellow solutions decrease with increasing temperature (Fig. 2a):

Figure 2b represents the electric susceptivity according to the inverse of the temperature square, for the aqueous solution 1% and 5% of Sunset Yellow and, respectively, for H_2O.

The linear dependence of the electric susceptivity (χ) on the inverse of the temperature square [22, 42, 43], for aqueous solutions of Sunset Yellow with concentrations of 0%

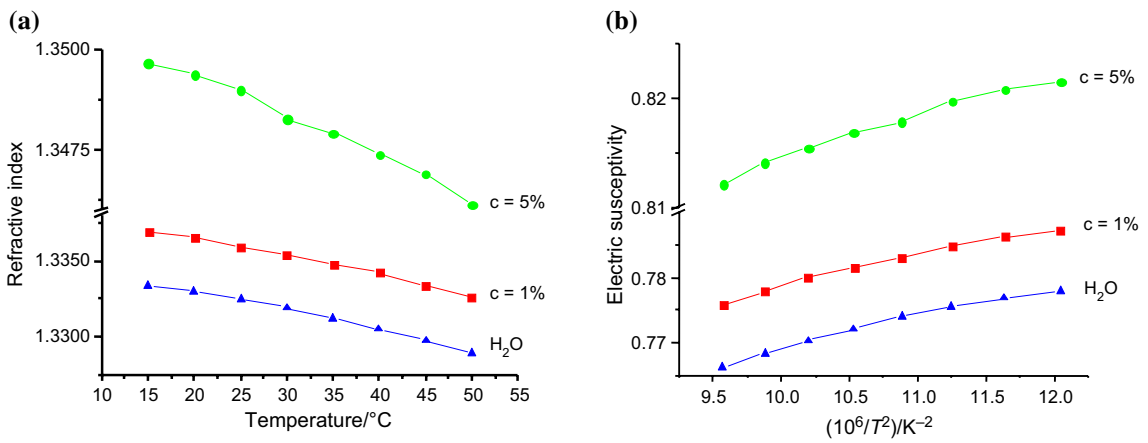

Fig. 2 **a** The refractive index as function of temperature and **b** the electric susceptivity represented as function of inverse square temperature (T^{-2}), (sigmoidal fit) for the aqueous solutions of Sunset Yellow with concentrations of 1% and 5%, and for H_2O

(H_2O, distilled water), 1% and 5% is exemplified through relationships (1–3):

$$\chi_{H_2O} = 0.72124 + 4794\left(\frac{1}{T^2}\right) \quad (1)$$

$$\chi_{1\%\ \text{Sunset Yellow}} = 0.732312 + 4631\left(\frac{1}{T^2}\right) \quad (2)$$

$$\chi_{5\%\ \text{Sunset Yellow}} = 0.776069 + 3836\left(\frac{1}{T^2}\right) \quad (3)$$

The refractive index and the electric susceptibility of Sunset Yellow's aqueous solutions are correlated with dye's purity (the purity is specified as not less than 85% total colouring matters) [1].

Using the refractive indices of the Sunset Yellow solutions, the dielectric constant (ε_r), $\varepsilon_r = n^2$, and the electric susceptivity (χ_e), $\chi_e = \varepsilon_r - 1$, were calculated.

The electric susceptivity is expressed by Eq. 4:

$$\chi_e = \varepsilon_r - 1 = N_1\left(\alpha_1 + \frac{p_0^2}{3\varepsilon_0 kT}\right) + N_2(\alpha_+ + \alpha_-) \quad (4)$$

In Eq. (4), N_1 is the number of water molecules, which is temperature dependent and have the electric polarizability α_1, N_2^+ is the number of positive ions of aqueous Sunset Yellow solutions with electric polarizability α_+, and N_2^- is the number of negative ions of aqueous Sunset Yellow solutions with electric polarizability α_-, where $N_2^+ = N_2^- = N_2$ [22, 42, 43]. Also in Eq. (4), p_0 is the electric dipole moment of Sunset Yellow, $\varepsilon_0 = 8.854 \times 10^{-12}$ F m^{-1} is absolute permittivity of vacuum, and $k = 1.38 \cdot 10^{-23}$ J K^{-1} is Boltzmann constant.

Optical anisotropy of Sunset Yellow

When drying at room temperature of the Sunset Yellow aqueous solutions with concentrations of $c = 1\%$ and $c = 5\%$ were obtained the crystals which were analyzed with the polarized light microscope. Results indicated that Sunset Yellow is an anisotropic azo dye (Figs. 3, 4). It has non-uniform spatial distribution of properties depend of the direction of the incident light. During a 360° rotation of the rotating holder of the microscope (α is the angle of the microscope's rotating holder), the section alternately shows four extinction positions and four of illumination, so the sample is anisotropic dye [13, 26, 34, 37, 38, 43].

The phenomenon of birefringence or double refraction, which is based on the laws of electromagnetism, is obtained in Sunset Yellow's crystals. Light switch-off positions and positions in which the crystals have a maximum brightness are obtained [37, 38]. Optical anisotropy is a phenomenon correlated with the light absorption, with the development of the colour [26, 34], and probably with the Sunset Yellow's intense the antioxidant activity, with he's low level of phytotoxicity and with an fertilization effect at wheat grains growth, how we observed in the study of biological activity of Sunset Yellow (antioxidant activity and its phytotoxicity) from this paper.

Fourier transform infrared (FTIR) spectroscopy of Sunset Yellow

FTIR measurements of Sunset Yellow were effectuated on the wavenumbers domain: 4000–550 cm^{-1} with a resolution of 4 cm^{-1} (Fig. 5). The representation of the Sunset Yellow spectrum is in the absorbance mode.

Table 1 shows the wavenumbers of the Sunset Yellow absorption maxima, with the assignment of the bonds to which they refer [16, 17, 42–50]:

The FTIR spectrum of Sunset Yellow [16, 17, 42–50] reveals intense specific bands at 1504, 1176, 1117, 1030, 1005, 984, 898, 832, 801, 745, 707, 693, 669, 641, 633, 599, 573 and 562 cm^{-1} which are related to N=N, sodium 1-naphthalenesulfonate ($C_{10}H_7NaO_3S$), $SO_3^-M^+$ (Na^+), C_6H_5-, $-C_6H_4-$, $C_{10}H_7-R$, >S=O, C–S, C–H and $R-C_6H_4-R_1$ groups.

The typical bands are related to azo group (–N=N–), which gives signals at 1504 cm^{-1}, 1476 cm^{-1} and at 1415 cm^{-1} (Table 1).

The Raman spectrum of Sunset Yellow

The Raman spectrum of Sunset Yellow powder is shown in Fig. 6. The positions of the intensities of the Raman displacements for Sunset Yellow are shown in Table 2, where an assignment of the most characteristic vibrations is also presented:

UV–Vis absorption spectrum of Sunset Yellow

The UV–Vis absorption spectrum of Sunset Yellow was obtained by using the Ocean Optics S2000 UV–Vis spectrophotometer. The sample was a Sunset Yellow's aqueous solution of 0.0025% concentration and used a 10 mm thick cuvette. In UV–Vis absorption spectrum of Sunset Yellow, an absorption band with a peak at $\lambda = 482.47$ nm is observed (Fig. 7).

The absorbance at this wavelength is 0.785. The experimentally established wavelength (located in the absorption band of E110), which is closest to the wavelength of $\lambda = 476.50$ nm (radiation emitted by the Ar + laser), was $\lambda = 476.48$ nm with the absorbance of 0.770. For this absorbance, which is about 98% of the absorbance at $\lambda = 482.47$ nm,

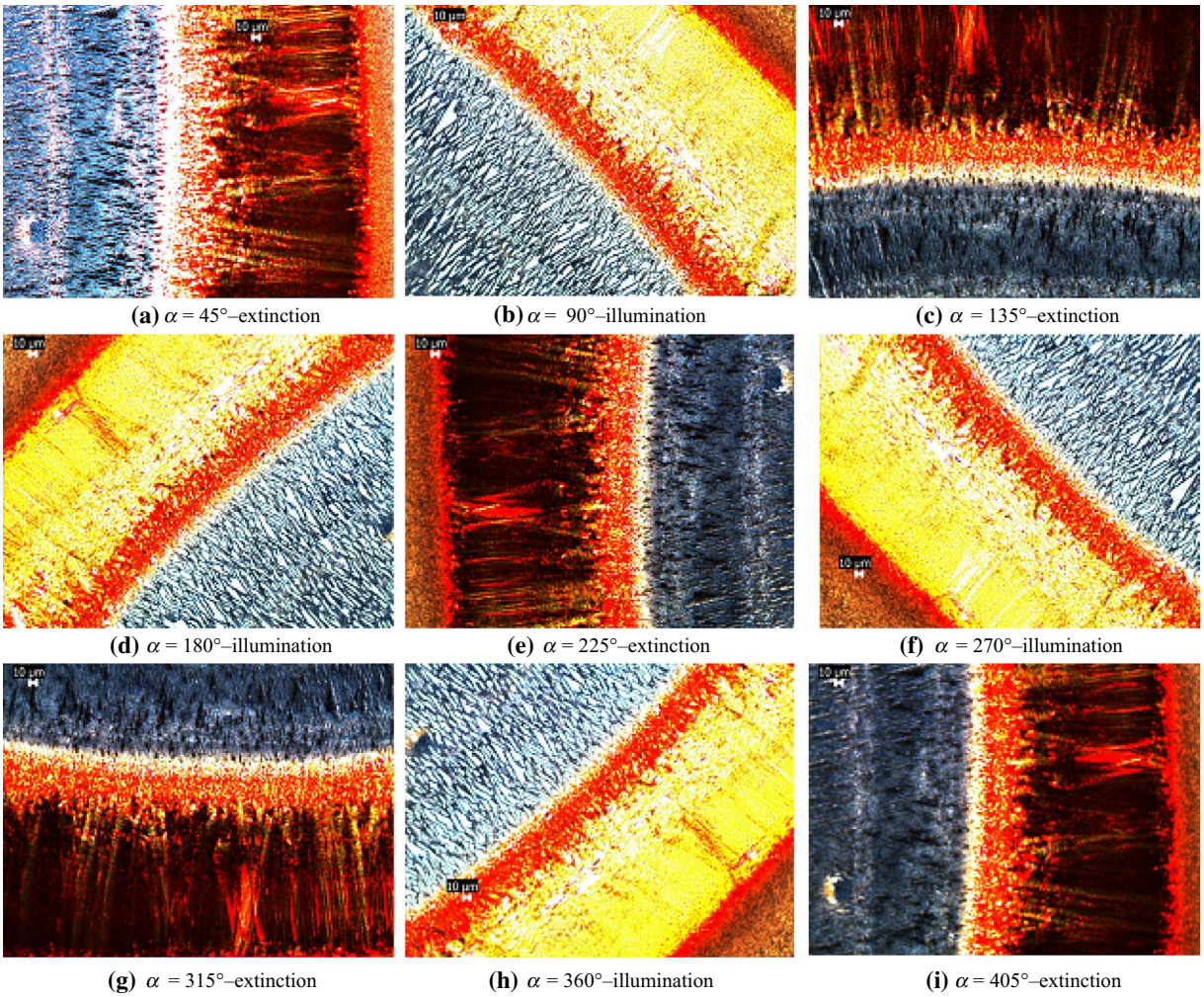

Fig. 3 Images of Sunset Yellow crystallites obtained by drying a solution with $c = 1\%$; segment value = 10 μm; the sample holder was rotated in trigonometric sense with a step of 45°

it can be concluded that Sunset Yellow has a good quantum efficiency for laser fluorescence at $\lambda = 476.50$ nm [34].

Fluorescence of Sunset Yellow

Sunset Yellow shown a laser fluorescence spectrum. The power of the excitation radiation source ($\lambda = 476.5$ nm) is 440 mW and was measured using a Coherent Max Field Top 2 power meter. The cuvete is made of quartz and has a thickness of 10 mm. The fluorescence spectra were recorded with an optical fibre positioned perpendicular to the excitation beam. The optical fibre is coupled to the spectrometer, which is connected to the computer. From these graphs, using the NIST Atomic Database [51, 52], in the wavelengths corresponding to de-excitation radiation, respectively, the spectral lines of the transitions between the energy levels of the chemical elements in the studied Sunset Yellow, were determined. Determining of the wavelengths of the fluorescence radiation has the accuracy of ±0.31 nm.

Sunset Yellow is an azo dye for which, in the aqueous solution with $c = 5\%$ concentration, the laser fluorescence spectrum of Fig. 8 was obtained.

The wavelengths of de-excitation radiation for Sunset Yellow, respectively the energies corresponding to the energy levels involved in the transitions and the electronic configurations related to them [51, 52], are summarized in the Tables 3–7.

The energies corresponding to the energy levels involved in the transitions and the electronic configurations corresponding to these levels, respectively, the radiation wavelengths at the transition from the superior level, to the inferior level (of de-excitation) [42, 43, 51, 52], are summarized in Tables 3–7. Sometimes electronic transitions occur at the same wavelength, of several elements (ions). Therefore, the electronic transitions between the energy levels in

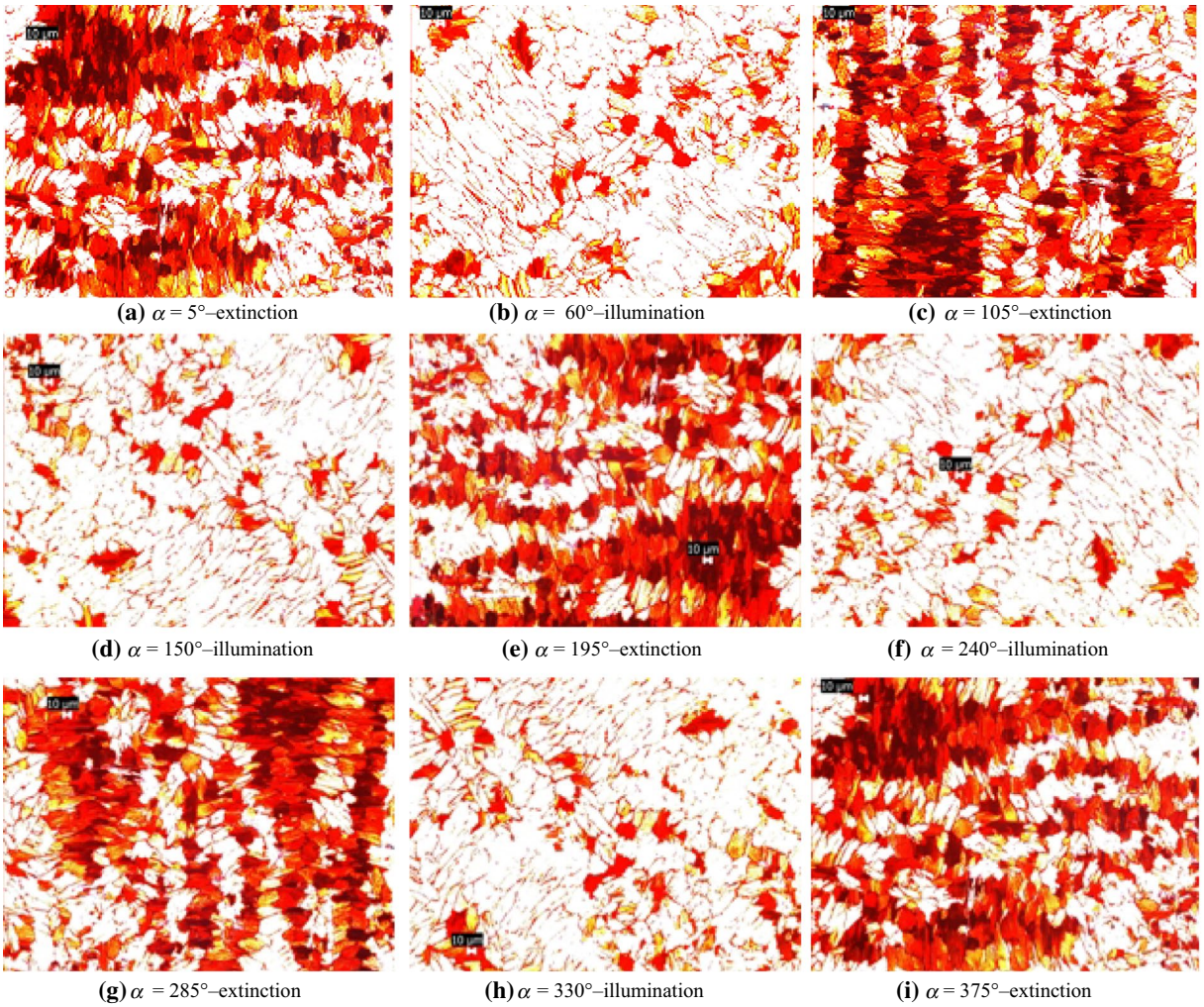

Fig. 4 Images of Sunset Yellow crystallites obtained by drying a solution with $c = 5\%$; segment value = 10 µm; the sample holder was rotated in trigonometric sense with a step of 45°

Tables 3–7 are systematized in Table 8, according to the wavelength of the emitted radiation.

The laser fluorescence lines of sunset yellow are intense and are in agreement with those of databases and experimental ones obtained by other authors [51, 52]. Table 8 confirms the finding that some laser fluorescence spectral lines may belong to the fluorescence of two or more chemical elements. There are also fluorescence spectral lines that are emitted by a single element, after which the element can be identified: carbon at 706.49 (w) and at 827.09 (w), oxygen at 738.34 (s), sulphur at 827.09 (w). The electronic transitions from the wavelengths of 612.14 (s), 617.51 (vs), 640.21 (w), 664.36 (vs), 686.98 (s), 697.08 (w), 750.77 (vs), 611.80 nm (s), 617.51 nm (m) and 750.77 nm (w) are thus attributed to the fluorescence of several elements (ions), which explains the high intensity of certain spectral lines of fluorescence.

The THz spectrum of Sunset Yellow

The THz spectroscopy investigation of the Sunset Yellow compound was conducted in a LabVIEW program. The experiments were recorded at ambient conditions of temperature and humidity; also, the sample temperature was monitored [41].

By identifying the characteristic absorption frequencies of the investigated substances, in different environments, a "signature" of the substance can be established, according to the characteristic frequencies of the radiation [26, 34, 41, 53–60]. The absorption spectra in the 0.2–4.5 THz range of Sunset Yellow were acquired for three forms: solid powder, 5% Sunset Yellow in aqueous solution, and the same solution impregnated in a porous paper that was subsequently dried at 105 °C.

Because water and paper absorb incident radiation over the entire frequency range used, water and paper absorption

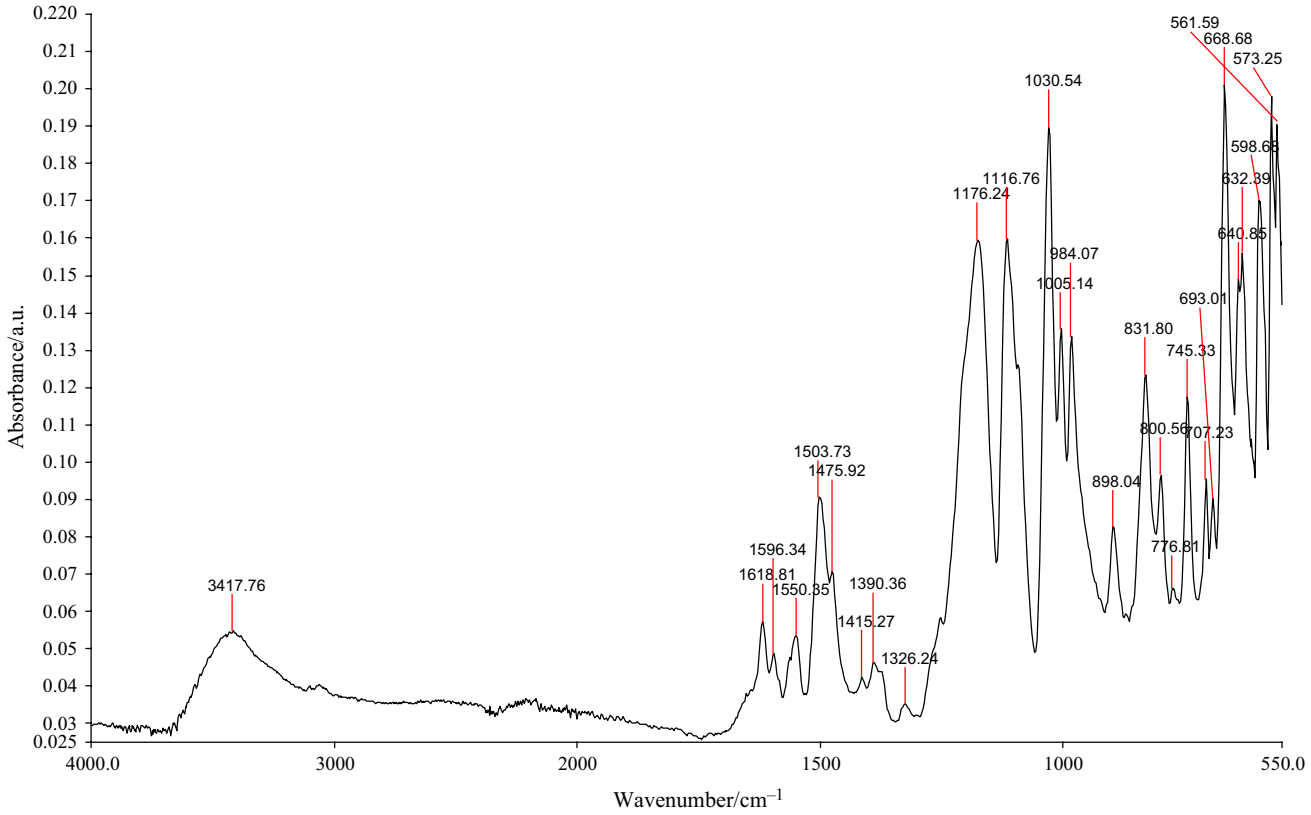

Fig. 5 FTIR spectrum of Sunset Yellow powder material

spectra were also recorded, which were removed by the software from the total spectra in order to only obtain curves for azo food dye Sunset Yellow.

The THz spectral signature of Sunset Yellow, obtained by processing numerical THz spectroscopy data, is shown in Table 9, where ν (THz) is the frequency of the Sunset Yellow sample transmission spectrum (0.2–4.5 THz) and the absorbance is the value for the corresponding frequency, for the three forms indicated above.

In Table 9, the bold digits represent the values obtained by THz spectroscopy, corresponding to the absorbance of the common peaks for the three forms of the Sunset Yellow (E110, A-E110, DP-E110), observed at the same frequency ν/THz; the other values in Table 9 are the significant values of the absorbances corresponding to the peaks in the three forms of the Sunset Yellow, in the proximity of the common peaks, ordered in increasing frequency. The THz spectral signature of Sunset Yellow consists of the absorption frequencies: 0.76, 1.61, 1.67, 1.74, 1.80, 2.01, 2.65 and 3.54 Tz.

Morphological characterization of Sunset Yellow

(a) Energy-dispersive X-ray spectroscopy (EDXS)

EDXS at beam energy of 15 keV was used to evaluate the chemical compositions of the Sunset Yellow's powder in 10 points (Fig. 9).

In interpreting the results in the points of Fig. 9, the placement of Sunset Yellow powder on the carbon support must be taken into account. The particularly high value of the average percentage of carbon identified experimentally (66.98% by mass), compared to the value of the percentage of carbon calculated from the chemical formula of Sunset Yellow of 42.44% (by mass), is explained by the uneven distribution of crystals on the carbon support (see Table 10).

In Table 10, in addition to the elements contained in Sunset Yellow, in spectrum 1 appears the aluminum, from the production phase. Chlorine and potassium also appear in all 10 spectra. These elements come from sodium and potassium chlorides, which are allowed in small amounts [1].

(b) Scanning electron microscopy (SEM)

Table 1 Main infrared absorption maxima of Sunset Yellow and their assignments

Wavenumber (intensity*)/ cm^{-1}	Assignments
3417.76 (m)	–OH hydroxyl stretching vibrations;
1618.81 (m)	Aromatic ring C–C stretching vibrations; aromatic ring C=C stretching vibrations; polynuclear aromatic compounds, naphthalenes C=C stretching vibrations;
1596.34 (w)	Aromatic ring C–C stretching vibrations; aromatic ring C=C stretching vibrations; polynuclear aromatic compounds, naphthalenes C=C stretching vibrations;
1550.35 (m)	Aromatic ring C–C stretching vibrations; polynuclear aromatic compounds, naphthalenes C=C stretching vibrations;
1503.73 (s)	Aromatic ring C–C stretching vibrations; aromatic ring skeletal vibrations; aromatic ring C=C stretching vibrations; polynuclear aromatic compounds, naphthalenes C=C stretching vibrations; aromatic ring stretching vibrations; N=N stretchinh vibrations;
1475.92 (m)	Aromatic ring C–C stretching vibrations; aromatic ring C=C stretching vibrations; aromatic ring stretching vibrations; N=N stretching vibrations;
1415.27 (w)	CH; aromatic azo compounds in the trans form;
1390.36 (w)	Polynuclear aromatic compounds, naphthalenes C=C stretching vibrations; polynuclear aromatic compounds, disubstituted naphthalenes;
1326.24 (vw)	Aromatic C–OH bending;
1176.24 (vs)	Sodium 1-naphthalenesulfonate ($C_{10}H_7NaO_3S$); aromatic = C–H in-plane deformation vibrations;
	Sulphonic acid salts, S03-M + (Na) asymmetric S03 stretching vibrations;
1116.76 (vs)	Sodium 1-naphthalenesulfonate ($C_{10}H_7NaO_3S$); aromatic = C–H in-plane deformation vibrations;
1030.34 (vs)	Sulphonic acid salts, S03-M + (Na) symmetric S03 stretching vibrations; aromatic C–H in- plane bending;
1005.14 (vs)	Aromatic = C–H in-plane deformation vibrations; aromatic C–H in-plane bending;
984.07 (vs)	Aromatic = C–H in-plane deformation vibrations; aromatic C–H in-plane bending;
898.04 (s)	2-monosubstituted naphthalenes, out-or-plane deformation vibrations (1 H)
831.80 (vs)	Para-disubstituted benzenes, aromatic C–H out-of-plane deformation vibrations; 2-monosubstituted naphthalenes, out-or-plane deformation vibrations (1 H);
	Substituted naphthalenes: characteristic C–H vibrations, two adjacent hydrogen atoms, out-of-plane vibrations;
800.56 (s)	Para-disubstituted benzenes, aromatic C–H out-of-plane deformation vibrations; polynuclear aromatic compounds, 1-monosubstituted naphthalenes C–H out-of-plane deformation vibrations (3H); substituted naphthalenes: characteristic C–H vibrations, two adjacent hydrogen atoms, out-of-plane vibrations;
776.81 (m)	Polynuclear aromatic compounds, 1-monosubstituted naphthalenes C–H out-of-plane deformation vibrations (3H);
745.33 (vs)	C6H5–, –C6H4–, C10H7–R; C–H out-of-plane vibration of the aromatic ring; monosubstituted naphthalene's out-of-plane deformation vibrations (4H);
707.23 (s)	Sulphoxides > S=O, C–S stretching vibrations;
693.01 (s)	Sulphoxides > S=O, C–S stretching vibrations;
668.68 (vs)	Sulphoxides > S=O, C–S stretching vibrations;
640.85 (vs)	Aromatic ring deformation vibrations, in-plane ring deformation vibrations;
	Polynuclear aromatic compounds, in-plane ring vibrations;
632.39 (vs)	aromatic ring deformation vibrations, in-plane ring deformation vibrations;
	Polynuclear aromatic compounds, in-plane ring vibrations;
598.68 (vs)	O–H out-of-plane vibration;
573.25 (vs)	R–SO3–Na + ; O–H out-of-plane vibration; aromatic ring out-of-plane bending;
561.59 (vs)	R–C6H4–R1

*_vs_ very strong, _s_ strong, _m_ medium, _w_ weak, _vw_ very weak

The SEM images of Sunset Yellow are presented in Fig. 10a–g; the scanning electron microscope has registered the images at an accelerating voltage of 2 kV and 8200–9800 nA intensity of the emission electric current, allowing for magnifications between 1000× and 5000× and a scale detail of 10–50 µm.

From the SEM images, it is found that the Sunset Yellow powder contains well-formed crystallites, with the visible crystallization planes and with the dispersion between 5 and 20 µm. Figure 10a–c shows the same points from the surface, at different magnifications and the same in Fig. 10d, e—from other points on the surface of the sample.

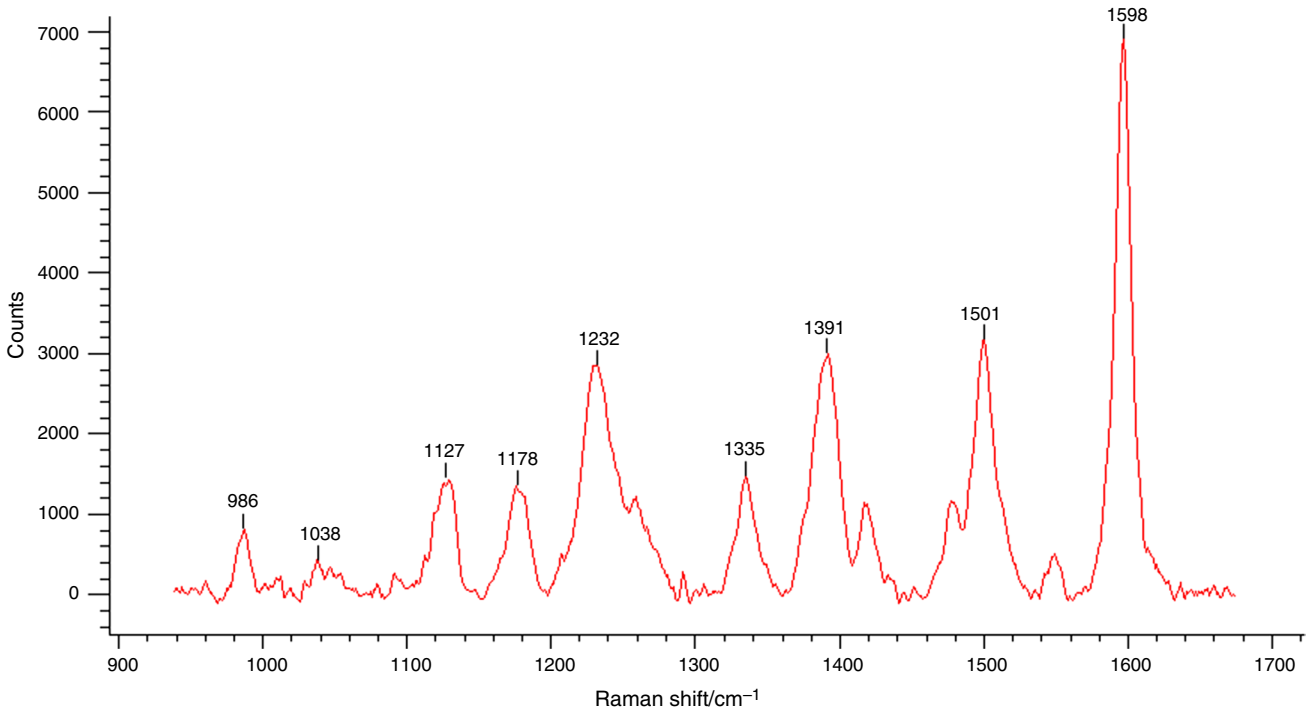

Fig. 6 The Raman spectrum of Sunset Yellow

Table 2 Raman shift of Sunset Yellow and assignments [42–45, 48–50]

Raman shift (Intensity*)/ cm^{-1}	Assignment (**)
1598 (vs)	Stretching (p.r.2); in-plane C–H deformation (p.r.2); stretching (OH); aromatic ring stretching vibration; naphthalenes stretching vibration; the stretching vibration of the C–C;
1501 (s)	The stretching vibration of the C–C;
1391 (s)	Associated phenol interaction of O–H def., C–OH bending vibration; O–H deformation vibration and C–O stretching of phenols; 1,4 disubstituted benzenes aromatic = C–H in-plane deformation vibrations;
1335 (m)	Stretching (–C–N=N–C–); associated phenol interaction of O–H def., C–OH bending vibration; O–H deformation vibration and C–O stretching of phenols
1232 (s)	Stretching asymmetric (C–N); phenols O–H deformation vibration; aromatic C–H in-plane deformation vibration; O–H deformation vibration and C–O stretching of phenols; asymetric SO_3 stretching vibration; 1,4 disubstituted benzenes aromatic = C–H in-plane deformation vibrations;
1178 (m)	Asymetric SO_3 stretching vibration;; aromatic C–H in-plane deformation vibrations; 1,4 disubstituted benzenes aromatic = C–H in-plane deformation vibrations;
1127 (m)	out-of-plane C–H def. (p.r.2); bending (p.r.2); stretching C–N; in-plane deformation vibrations of aromatic C–H bonds; 1,4 disubstituted benzenes aromatic = C–H in-plane deformation vibrations;
1038 (vw)	Symetric SO_3 stretching vibration; aromatic C–H in-plane deformation vibrations;
986 (w)	Aromatic C–H in-plane deformation vibration; 1,4 disubstituted benzenes aromatic = C–H in-plane deformation vibrations;

**vw* very weak, *w* weak, *m* medium; *s* strong; *vs* very strong

***ν* stretching, *δ* bending, *ρ* rocking, *wagg.* wagging, *p.r.2* phenyl ring bonding at azo group, *s* symmetric, *as* asymmetric, *def.* deformation, *op* out-of-plane

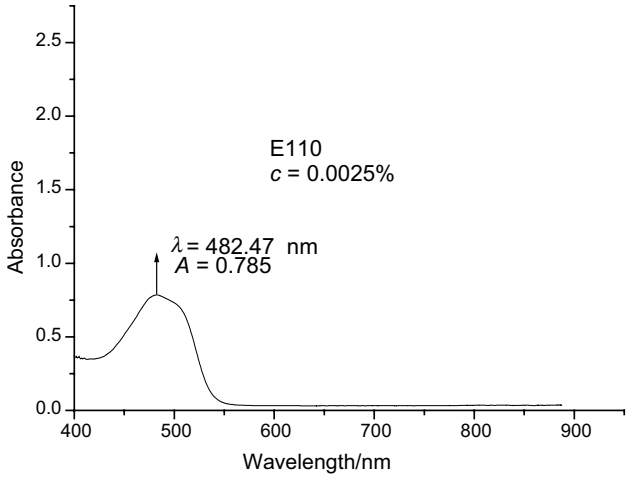

Fig. 7 UV–Vis spectrum of Sunset Yellow

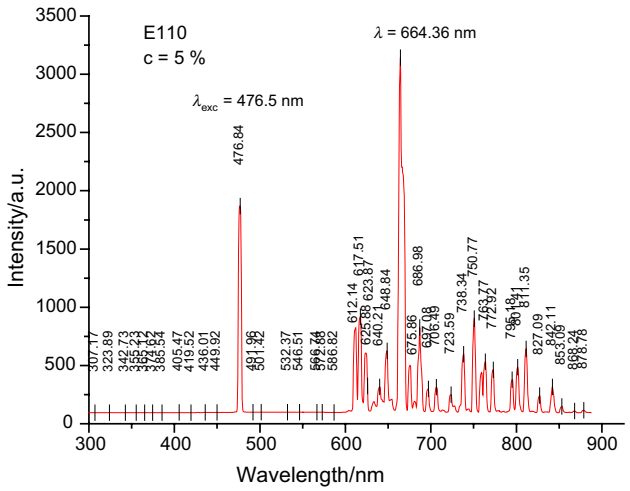

Fig. 8 Fluorescence spectrum of aqueous of Sunset Yellow's solution with concentration $c = 5\%$

Thermal analysis and calorimetry study of Sunset Yellow

The thermal investigation of Sunset Yellow was performed in the temperature range RT–1000 °C [11, 26, 34, 42, 43, 61–65]. The Sunset Yellow powder was heated-up in dynamic air atmosphere (150 cm^3 min^{-1}) with a heating rate of 10 °C min^{-1}; the thermoanalytic curves (TG, DTG and DSC) are shown in Fig. 11.

These curves indicate a 4-step oxidative behaviour: 3 steps of oxidative decomposition and 1 step of burning; the results are summarized in Table 11.

Thermal analysis and calorimetry study performed in air indicates the removal of absorbed water molecules up to 188 °C, after which the Sunset Yellow compound exhibits a good thermal stability up to 330 °C.

In the temperature range 330–406 °C, a moderate exothermic effect is observed (thermal effect 1, from Fig. 12), which consists in the loss of C_3H_2 group, while between 460 and 510 °C, the weak exothermic effect (thermal effect 2, from Fig. 12) stands for the loss of the HCN group.

In the temperature range 512–616 °C, a major exothermic effect was observed (effect 3, from Fig. 13), with the loss of $C_{10}H$, HCl and SO_3 groups, of $\Delta H = -4519.6$ J g^{-1}, while between 827 and 920 °C a major thermal exothermic effect (effect 4, from Fig. 14) happens with the burning of the formed polycondensed carbonaceous groups (tars), of $\Delta H = -1453.41$ J g^{-1}.

The exact mass loss stages for the water removal and the oxidative decompositions of Sunset Yellow are shown in Fig. 15.

The residue is Na_2SO_4 (sodium sulphate) and Na_2C_2 (disodium acetylide/sodium carbide), with a theoretical percentage of 31.77% and practically 31.51% (Fig. 15). The groups of evolved/formed atoms were assumed, based on the experimental mass losses.

The results of the thermal analysis confirm the chemical formula and composition of the Sunset Yellow food azo dye: $C_{16}H_{10}N_2Na_2O_7S_2$, with NaCl traces and absorbed H_2O.

Following the thermal and calorimetric study of Sunset Yellow, it was established that the maximum temperature at which a food—containing this dye—can be thermally processed is 330 °C. However, between 188 and 330 °C, it is recommended for the foods containing Sunset Yellow, to thermally process those in an oxygen-poor atmosphere, preferably in closed containers.

Acidity study of the Sunset Yellow

The pH measurements of Sunset Yellow, as a function of temperature, were made using distilled water as reference, starting from room temperature (RT), to approximately 55 °C [66].

The temperature-dependent pH measurements for the aqueous Sunset Yellow solution, with 1% concentration, are shown in Fig. 16a.

The Sunset Yellow solution has, at temperature of 24 °C, an acid character, corresponding to a pH = 6.28, and as the temperature increases, the acidity of the sample increases, the *pH* reaching a value of 6.15 at temperature of 57 °C.

Table 3 Atomic fluorescence of the carbon from 5% Sunset Yellow solution in water [51, 52]

Ion	*Wavelength* measured (in air) λ/nm ± 0.31 nm	*Wavelength* from the literature (in air) λ/nm	*Wavelength* calculated Ritz (in air) λ/nm	Energy of the superior level E_k/eV	Energy of the inferior level E_i/eV	The electronic configuration of the superior level	The electronic configuration of the inferior level
C I	612.14	612.0818	612.0815	10.8757181	8.85066275	$2s^22p7s$	$2s^22p3p$
C I	623.87	623.7265	623.7257	10.989834	9.00258374	$2s^22p(^2P°_{3/2})7d$	$2s^22p3p$
C IV	640.21	–	640.450	61.78327	59.84792	$1s^29p$	$1s^27s$
C IV		–	640.495	61.78314	59.84792	$1s^29p$	$1s^27s$
C III	686.98	–	686.878	41.864006	40.059463	$1s^22p(^2P°)3d$	$1s^22p(^2P°)3p$
C III		–	687.053	42.679860	40.875777	$1s^22s5p$	$1s^22p(^2P°)3p$
C III		–	687.204	41.867981	40.064294	$1s^22p(^2P°)3d$	$1s^22p(^2P°)3p$
C I	697.08	–	697.02882	10.41865831	8.64039597	$2s^22p4d$	$2s^22p3p$
C II	706.49	–	706.368	24.653514	22.898763	$2s2p(^3P°)3d$	$2s2p(^3P°)3p$
C I		–	706.589939	10.39459617	8.64039597	$2s^22p4d$	$2s^22p3p$
C II	723.59	723.642	723.642	18.045987	16.333123	$2s^23d$	$2s^23p$
C II		–	723.717	18.045809	16.333123	$2s^23d$	$2s^23p$
C I	750.77	750.567	750.567	10.981887	9.33046719	$2s^22p(^2P°_{1/2})7f$	$2s2p^3$
C II			750.889	22.570506	20.919795	$2s2p(^3P°)3p$	$2p^3$
C I	763.77	–	763.492536	10.39459617	8.77113462	$2s^22p4d$	$2s^22p3p$
C III		–	763.497	39.849923	38.226472	$1s^22s4d$	$1s^22p(^2P°)3s$
C IV	772.92	772.62	–	–	–	–	–
C I	801.41	801.498	801.50251	10.39459617	8.84812431	$2s^22p4d$	$2s^22p3p$
C III	827.09	–	827.204	42.836187	41.337763	$1s^22s5d$	$1s^22p(^2P°)3d$
C III		–	827.233	42.836134	41.337763	$1s^22s5d$	$1s^22p(^2P°)3d$
C V	842.11	–	842.072	353.5342	352.06228	1s3p	1s3s

Table 4 Atomic fluorescence of the oxygen from 5% Sunset Yellow solution in water [51, 52]

Ion	*Wavelength* measured (in air) λ/nm ± 0.31 nm	*Wavelength* from the literature (in air) λ/nm	*Wavelength* calculated Ritz (in air) λ/nm	Energy of the superior level E_k/eV	Energy of the inferior level E_i/eV	The electronic configuration of the superior level	The electronic configuration of the inferior level
O IV	617.51	–	617.227	73.5730	71.5648	$2s2p(^3P°)4d$	$2p^2(^3P)3s$
O II	648.84	648.6461	648.6462	33.621024	31.7101220	$2s^22p^2(^3P_1)6g$	$2s^22p^2(^3P)4f$ G
O II	664.36	664.1054	664.1031	25.2856209	23.4191944	$2s^22p^2(^3P)3p$	$2s^22p^2(^3P)3s$
O IV		–	664.445	73.3861	71.5207	$2s2p(^3P°)4d$	$2p^2(^3P)3s$
O II		664.6350	664.6357	33.622638	31.7577075	$2s^22p^2(^3P_1)6$ g	$2s^22p^2(^3P)4f$ F
O II	686.98	686.9485	686.9475	30.4881139	28.6837549	$2s^22p^2(^3P)4p$	$2s^22p^2(^3P)3d$
O II	738.34	–	738.0307	30.5362939	28.8568237	$2s^22p^2(^3P)4p$	$2s^22p^2(^3P)3d$
O II		738.1118	738.1168	30.5362939	28.8570197	$2s^22p^2(^3P)4p$	$2s^22p^2(^3P)3d$
O II		738.3744	738.3758	33.052740	31.374055	$2s^22p^2(^1D)4p$	$2s^22p^2(^1D)3d$
O II	801.41	801.3157	801.3160	31.367182	29.820351	$2s^22p^2(^1S)3p$	$2s^22p^2(^1S)3p$
O II		–	801.712	31.366419	29.820351	$2s^22p^2(^1S)3p$	$2s^22p^2(^3P)4s$

From the *pH* value of the Sunset Yellow solution, the concentration of hydrogen ions is calculated Fig. 16b.

The concentration of hydrogen ions $[H^+]$ increases with increasing temperature, from the value of $5.22 \cdot 10^{-7}$ mol L^{-1}, corresponding to the temperature of 23.7 °C, to the value of $7.16 \cdot 10^{-7}$ mol L^{-1} at the temperature of 57.42 °C.

Table 5 Atomic fluorescence of the sulphur from 5% Sunset Yellow solution in water [51, 52]

Ion	*Wavelength* measured (in air) λ/nm ± 0.31 nm	*Wavelength* from the literature (in air) λ/nm	*Wavelength* calculated Ritz (in air) λ/nm	Energy of the superior level E_k/eV	Energy of the inferior level E_i/eV	The electronic configuration of the superior level	The electronic configuration of the inferior level
S II	612.14	612.3383	612.3395	16.091640	14.067438	$3s^23p^2(^3P)4p$	$3s^23p^2(^3P)4s$
S I	617.51	617.277	617.277	10.053218	8.0452061	$3s^23p^3(^4S°)7d$	$3s^23p^3(^4S°)4p$
S I		617.361	617.361	10.052944	8.0452061	$3s^23p^3(^4S°)7d$	$3s^23p^3(^4S°)4p$
S I		–	617.369	10.053218	8.0455064	$3s^23p^3(^4S°)7d$	$3s^23p^3(^4S°)4p$
S I		–	617.415	10.053218	8.0456547	$3s^23p^3(^4S°)7d$	$3s^23p^3(^4S°)4p$
S I		617.497	617.499	10.052944	8.0456547	$3s^23p^3(^4S°)7d$	$3s^23p^3(^4S°)4p$
S I		617.582	617.582	10.052675	8.0456547	$3s^23p^3(^4S°)7d$	$3s^23p^3(^4S°)4p$
S II	623.87	–	624.067	18.086525	16.100362	$3s3p^4$	$3s^23p^2(^3P)4p$
S I	640.21	640.358	640.357	9.801948	7.8663094	$3s^23p^3(^4S°)7s$	$3s^23p^3(^4S°)4p$
S II	664.36	664.106	664.1003	16.100362	14.233928	$3s^23p^2(^3P)4p$	$3s^23p^2(^3P)3d$
S I	675.86	–	675.675	9.704366	7.8699033	$3s^23p^3(^4S°)5d$	$3s^23p^3(^4S°)4p$
S I		–	675.696	9.704308	7.8699033	$3s^23p^3(^4S°)5d$	$3s^23p^3(^4S°)4p$
S I		675.716	675.715	9.704256	7.8699033	$3s^23p^3(^4S°)5d$	$3s^23p^3(^4S°)4p$
S VI	697.08	–	697.0	79.5521	77.7737	$2p^68p$	$2p^67d$
S IV			697.33	43.65325	41.87575	$3s3p(^3P°)4f$	$3s3p(^3P°)4d$
S II	723.59	723.7007	723.7018	15.867044	14.154321	$3s^23p^2(^3P)4p$	$3s^23p^2(^3P)3d$
S II	750.77	750.9066	750.9077	15.944264	14.293594	$3s^23p^2(^3P)4p$	$3s^23p^2(^3P)3d$
S II	801.41	801.2113	801.2100	18.086525	16.539488	$3s3p^4$	$3s^23p^2(^3P)4p$
S II	811.35	–	811.203	15.761906	14.233928	$3s^23p^2(^1D)3d$	$3s^23p^2(^3P)3d$
S II	842.11	–	842.140	16.539488	15.067641	$3s^23p^2(^3P)4p$	$3s^23p^2(^1D)4s$
S II		842.2300	842.2321	16.539488	15.067802	$3s^23p^2(^3P)4p$	$3s^23p^2(^1D)4s$

Table 6 Atomic fluorescence of the nitrogen from 5% Sunset Yellow solution in water [51, 52]

Ion	*Wavelength* measured (in air) λ/nm ± 0.31 nm	*Wavelength* from the literature (in air) λ/nm	*Wavelength* calculated Ritz (in air) λ/nm	Energy of the superior level E_k/eV	Energy of the inferior level E_i/eV	The electronic configuration of the superior level	The electronic configuration of the inferior level
N IV	612.14	–	611.923	63.80818	61.78260	$1s^22s4d$	$1s^22p(^2P°_{1/2})3d$
N II	617.51	–	617.331	25.139688	23.131853	$2s^22p4p$	$2s^22p3d$
N II		–	617.434	27.661100	25.653600	$2s^22p6s$	$2s^22p4p$
N I	623.87	–	623.7672	13.9967295	12.0096115	$2s^22p^2(^3P)5d$	$2s^22p^2(^3P)3p$
N I		–	623.8587	13.9869695	12.0001428	$2s^22p^2(^3P)5d$	$2s^22p^2(^3P)3p$
N II	640.21	–	639.915	25.133347	23.196373	$2s^22p4p$	$2s^22p3d$
N I		–	640.2364	13.6860942	11.7500915	$2s^22p^2(^3P)4d$	$2s^22p^2(^3P)3p$
N I		–	640.5255	13.6880235	11.7528948	$2s^22p^2(^3P)4d$	$2s^22p^2(^3P)3p$
N III	648.84	–	648.784	41.26249	39.35199	$2s2p(^3P°)3d$	$2s2p(^3P°)3p$
N I		649.122	649.1222	13.6623957	11.7528948	$2s^22p^2(^3P)4d$	$2s^22p^2(^3P)3p$
N I	664.36	664.496	664.4962	13.6291688	11.7638463	$2s^22p^2(^3P)5s$	$2s^22p^2(^3P)3p$
N I		664.650	664.6503	13.6149816	11.7500915	$2s^22p^2(^3P)5s$	$2s^22p^2(^3P)3p$
N I	675.86	–	675.9198	13.6782740	11.8444769	$2s^22p^2(^3P)4d$	$2s^22p^2(^3P)3p$
N III		–	676.133	43.95618	42.12296	$2s^26d$	$2s2p(^3P°)3d$
N II	686.98	–	686.958	30.300731	28.496399	$2s2p^2(^4P)3d$	$2s2p^2(^4P)3p$
NI	697.08	–	697.3074	13.6149816	11.8374297	$2s^22p^2(^3P)5s$	$2s^22p^2(^3P)3p$
N II		–	697.356	27.431029	25.653600	$2s^22p5d$	$2s^22p4p$
N I	750.77	–	750.7609	13.6511355	12.0001428	$2s^22p^2(^3P)5s$	$2s^22p^2(^3P)3p$

Table 7 Atomic fluorescence of the sodium from 5% Sunset Yellow solution in water [51, 52]

Ion	*Wavelength* measured (in air) λ/nm ± 0.31 nm	*Wavelength* from the literature (in air) λ/nm	*Wavelength* calculated Ritz (in air) λ/nm	Energy of the superior level E_k/eV	Energy of the inferior level E_i/eV	The electronic configuration of the superior level	The electronic configuration of the inferior level
Na II	612.14	612.146	–	–	–	–	–
Na II	617.51	617.525	617.536	45.769846	43.76268	$2s^22p^5(^2P°_{3/2})6f$	$2s^22p^5(^2P°_{3/2})4d$
Na VI	640.21	–	640	117.831	115.893	$2s2p^2(^4P)3$ s	$2s^22p3d$
Na II		640.479	–	–	–	–	–
Na III	697.08	–	697.7	61.148022	59.368964	$2s^22p^4(^1D)3d$	$2s^22p^4(^1S)3p$
Na I	750.77	–	750.7464	3.7533215	2.10229715	$2p^64p$	$2p^63p$
Na I		–	751.0617	3.7526285	2.10229715	$2p^64p$	$2p^63p$

Table 8 Systematization of laser electronic fluorescence spectral lines of Sunset Yellow elements (ions)

The measured wavelength λ/nm (*Intensity**)	The element (the ion) from Sunset Yellow which exhibits fluorescence at a certain wavelength				
	C	N	Na	O	S
612.14 (s)	Yes	Yes	Yes	–	Yes
617.51 (vs)	–	Yes	Yes	Yes	Yes
623.87 (m)	Yes	Yes		–	Yes
640.21 (w)	Yes	Yes	Yes	–	Yes
648.84 (m)	–	Yes	–	Yes	–
664.36 (vs)	–	Yes	–	Yes	Yes
675.86 (m)	–	Yes	–	–	Yes
686.98 (s)	Yes	Yes	–	Yes	–
697.08 (w)	Yes	Yes	Yes	–	Yes
706.49 (w)	Yes	–	–	–	–
723.59 (w)	Yes	–	–	–	Yes
738.34 (s)	–	–	–	Yes	–
750.77 (vs)	Yes	Yes	Yes	–	Yes
763.77 (m)	Yes	–	–	–	–
772.92 (m)	Yes	Yes	–	–	–
801.41 (m)	Yes	–	–	Yes	Yes
811.35 (s)	–	–	–	–	Yes
827.09 (w)	Yes	–	–	–	–
842.11 (w)	Yes	–	–	–	Yes
853.09 (vw)	–	–	–	–	–

**vs* very strong, *s* strong, *m* medium, *w* weak, *vw* very weak

Thus, by heating the liquids containing the food dye Sunset Yellow, their *pH* reveal a slightly increase in their acid character.

Table 9 THz spectral signature of Sunset Yellow

No	ν/THz	Absorbance (Intensity*)		
		Powder	Solution	Solution impregnated in paper
1	0.67	1.46 (m)	0.21(w)	52.50 (s)
2	**0.76**	**5.96 (m)**	**0.16 (w)**	**21.10 (s)**
3	0.86	2.89 (m)	0.23 (w)	31.30 (s)
4	1.19	2.59 (m)	11.00 (s)	1.54 (m)
5	1.27	14.40 (s)	15.20 (s)	0.97 (w)
6	1.41	443.00 (vs)	29.40 (s)	59.70 (s)
7	1.54	5.99 (m)	20.20 (s)	15.40 (s)
8	**1.61**	**4.21 (m)**	**0.58 (w)**	**1.26 (m)**
9	**1.67**	**5.38 (m)**	**0.71 (w)**	**40.30 (s)**
10	1.70	5.38 (m)	141.00 (vs)	40.30 (s)
11	**1.74**	**101.00 (vs)**	**6.72 (m)**	**2.14 (m)**
12	**1.80**	**2.53 (m)**	**7.58 (m)**	**12.70 (s)**
13	**2.01**	**4.16 (m)**	**11.70 (s)**	**0.89 (w)**
14	2.15	27.70 (s)	243.00 (vs)	25.20 (s)
15	2.27	31.10 (s)	4.34 (m)	134.00 (vs)
16	2.31	0.17 (w)	2.06 (m)	99.50 (s)
17	2.47	0.54 (w)	20.00 (s)	13.50 (s)
18	**2.65**	**2.34 (m)**	**1.13 (m)**	**2.83 (m)**
19	2.72	30.70 (s)	38.80 (s)	32.80 (s)
20	2.84	25.10 (s)	14.20 (s)	3.86 (m)
21	2.96	15.60 (s)	2.21 (m)	15.80 (s)
22	3.10	2.39 (m)	15.30 (s)	2.53 (m)
23	3.43	173.00 (vs)	0.61 (w)	12.60 (s)
24	3.47	81.50 (s)	13.80 (s)	1.15 (m)
25	**3.54**	**4.89 (m)**	**1.76 (m)**	**1.73 (m)**
26	3.63	4.72 (m)	29.21 (s)	8.37 (m)
27	3.81	465.00 (vs)	7.02 (m)	4.80 (m)

(*)*vw* very weak, *w* weak, *m* medium, *s* strong, *vs* very strong

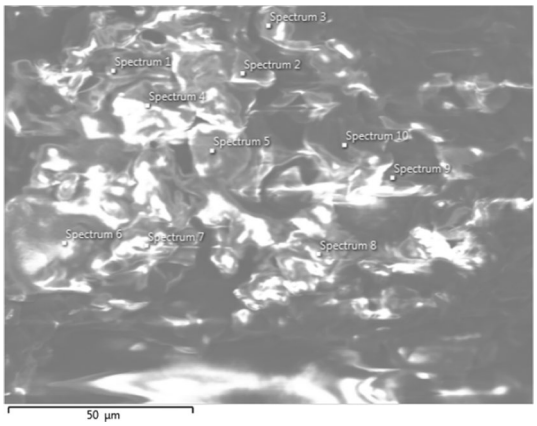

Fig. 9 SEM image of the Sunset Yellow's sample with the positions where the EDX spectra were acquired

Biophysical properties and biological activity of Sunset Yellow

(a) UV–Vis absorption spectra of bovine serum albumin (BSA) in interaction with Sunset Yellow

The interaction of food azo-dye E110 (Sunset Yellow) with BSA was analysed by UV–Vis spectroscopy with the UV–Vis Varian Cary 50 spectrophotometer (Fig. 17).

The electronic spectrum of bovine serum albumin shows a maximum at 280 nm due to the $\pi \rightarrow \pi^*$ transitions in the aromatic nuclei of the amino acid residues (tryptophan, tyrosine)—Fig. 17a. In the BSA—Sunset Yellow system, in the presence of increasing dye concentrations, from 1×10^{-5} M to 5×10^{-5} M, it is observed that the absorbance increases. The absorbance maximum has a hyperchromic effect and a hypochromic effect and shifts to shorter wavelengths, from 278 nm, in the case of the dye-free solution (Fig. 17a), to 275 nm in the case of the dye-containing solution in concentration of 5×10^{-5} M (Fig. 17g). Also in UV, absorbance maxima were observed at approximately 262 nm and 320 nm for curves **b–f**, and a displacement at 315 nm for curve **g**, and in the visible range, a maximum was observed at approximately 482 nm (Fig. 17). The displacement is due to the deployment of the protein and the change in the polarity of the environment around the aromatic amino acid residues in the protein structure [67, 68]. These observations prove that the protein can bind the dye to form a BSA-dye complex.

The absorption maximum at 482 nm obtained for Sunset Yellow is in good agreement with those mentioned in other works [50, 69], where in aqueous solution, a maximum was obtained at about 485 nm [69].

Shifting the maximum absorbance towards shorter wavelengths, when the concentration of Sunset Yellow increases, demonstrates that BSA can bind the dye and that bovine serum albumin can form a complex with Sunset Yellow [67, 68]. This can disrupt the normal biological function of bovine serum albumin.

(b) FTIR spectrum of collagen in interaction with Sunset Yellow

Table 10 The composition of the Sunset Yellow's powder in different areas of the surface, analysed by EDX spectroscopy

Result type	Mass%									
Statistics	C	O	Na	Al	S	Cl	K			
Max	91.08	24.03	11.95	0.09	24.85	1.41	9.83			
Min	57.48	4.84	0.99	0.09	1.59	0.08	0.49			
Average	66.98	11.78	4.79	–	11.31	0.73	4.4			
Standard Deviation	11.02	6.98	3.23	–	7.33	0.44	3.28			
Spectrum label	Spectrum 1	Spectrum 2	Spectrum 3	Spectrum 4	Spectrum 5	Spectrum 6	Spectrum 7	Spectrum 8	Spectrum 9	Spectrum 10
C	57.77	60.91	58.35	79.68	57.48	91.08	62.67	72.82	65.13	63.96
O	4.84	21	6.48	9.95	16.91	5.78	6.69	6.87	15.21	24.03
Na	1.25	7.92	5.11	3.18	11.95	0.99	4.88	4.87	3.08	4.67
Al	0.09	–	–	–	–	–	–	–	–	–
S	24.85	6.5	18.86	5.32	9.09	1.59	18.24	11.27	12.06	5.28
Cl	1.41	0.51	1.36	0.26	0.77	0.08	1.05	0.55	0.78	0.50
K	9.79	3.16	9.83	1.6	3.8	0.49	6.47	3.62	3.74	1.56
Total	100	100	100	100	100	100	100	100	100	100

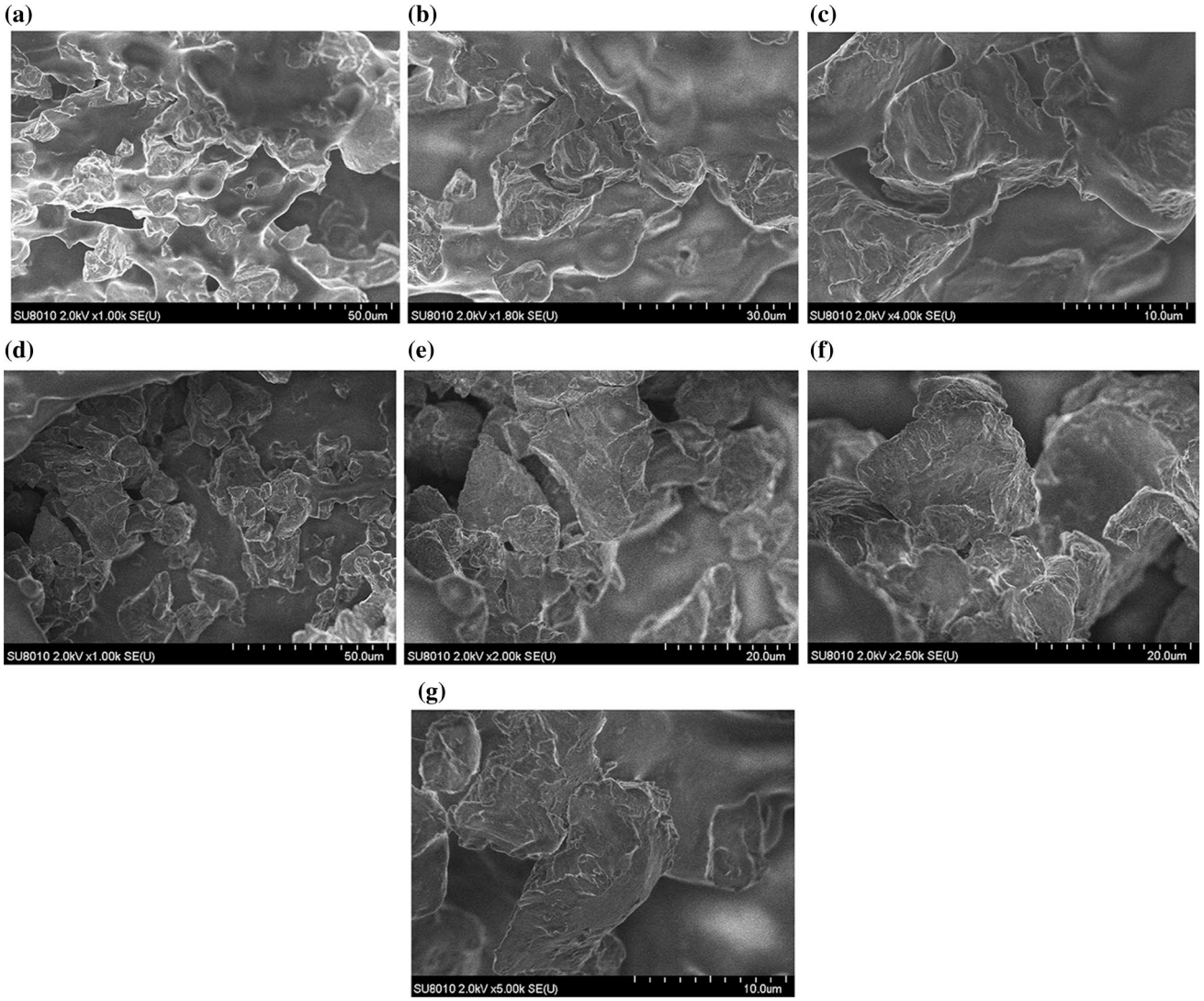

Fig. 10 SEM images of Sunset Yellow at magnifications of: **a** 1000×, **b** 1800×, **c** 4000×, **d** 1000×, **e** 2000×, **f** 2500×, **g** 5000×

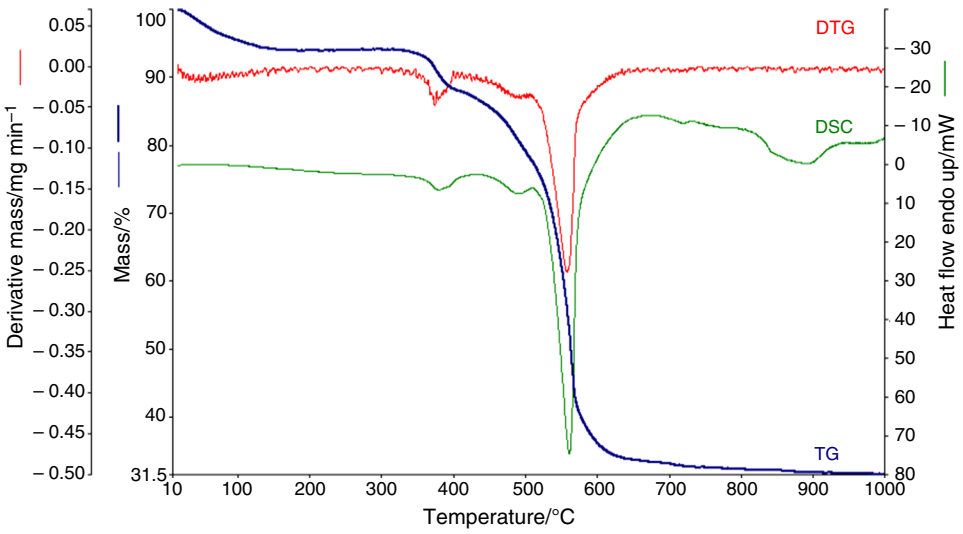

Fig. 11 Thermoanalytical curves (TG, DTG, DSC) of Sunset Yellow in air atmosphere, with 10 ºC min^{-1}

Table 11 Thermal parameters of Sunset Yellow determined by thermal analysis and calorimetry methods

Temperature range/°C	*Mass loss* (experimental)/%	*Mass loss* (theoretical)/%	Identified evolved/formed groups	ΔH/Jg^{-1}	Observations
RT–188	6.117	6.44	H_2O	0	Absorbed and physically bonded water. No thermal effect
330–430	6.99	6.8	C_3H_2	− 268.6	Moderate exothermic effect
430–510	9.22	9.66	2·HCN	− 62.2	Weak exothermic effect
510–643	42.52	43.88	$C_{10}H$, HCl, SO_3	− 4519.6	Major exothermic effect
643–920	2.03	2.86	Gudrons	− 1453.4	Major exothermic effect

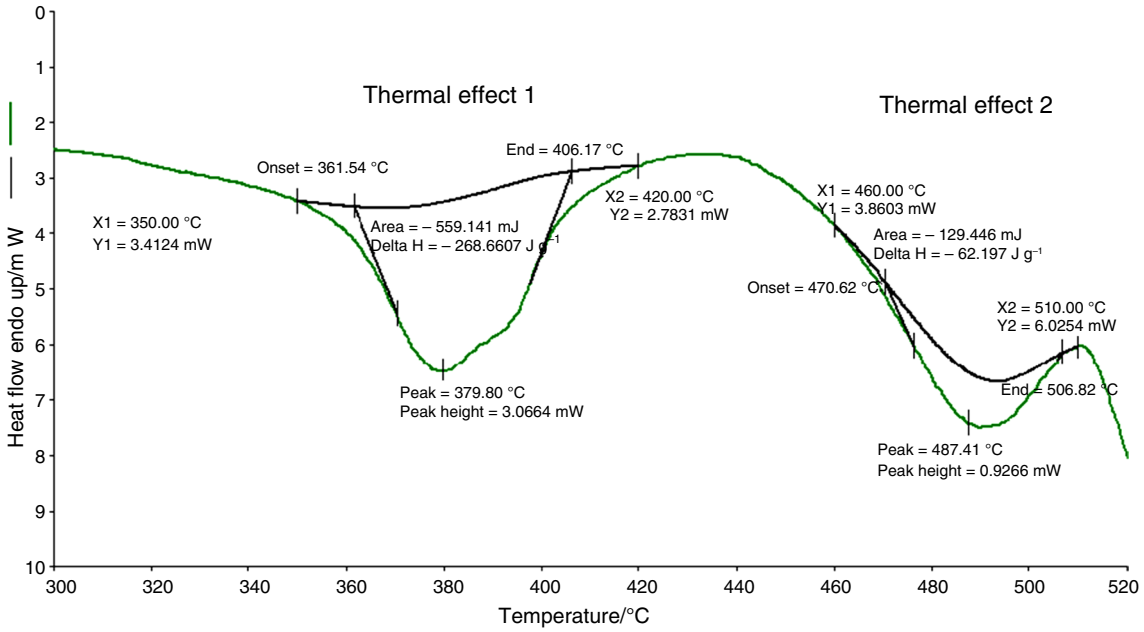

Fig. 12 Thermal effects 1 and 2 of the decomposition of Sunset Yellow in air atmosphere with 10 °C min^{-1}

The interaction of food dyes with collagen [45, 70] can be studied by FTIR spectroscopy. Sunset Yellow belongs to the azoic group of dye compounds, from which, by the interaction with the environment where they are processed and employed, is possible formation of carcinogenic aromatic amines and amides [1, 71–80].

In this paper, the interaction of skin collagen with Sunset Yellow was studied, through the FTIR spectrum of natural skin samples, treated or untreated with food azo dye solutions with 5% concentration. Figure 18 shows the FTIR spectrum of treated (a) and untreated (b) skin with 5% aqueous Sunset Yellow solution. The FTIR Bruker ATR Zn-Se spectrometer was used.

The characteristic vibrations of the amide bands I and II appear at 1651 cm^{-1} and 1549 cm^{-1}, respectively, which is in agreement which other papers [26, 34, 42, 43, 70]. The molecular arrangement and folding of proteins depend on the nature of the hydrogen bonds, and the interaction of collagen with Sunset Yellow is evidenced in its FTIR spectrum [45, 70]. In the presence of Sunset Yellow, the position of amide I band (C=O stretching) is at 1651.35 cm^{-1}, while the position of amide II band (NH bending and CN stretching) moved from 1540.17 to 1555.51 cm^{-1}. The spectral images show the changes produced by the interaction of collagen with Sunset Yellow and the influence of hydrogen bonds on the characteristics of NH peptide bonds [78–80]. These changes can have an undesirable effect on the structure of collagen and pose a potential risk to the skin.

(c) Determination of the antioxidant activity of Sunset Yellow, by the Folin–Ciocâlteu method

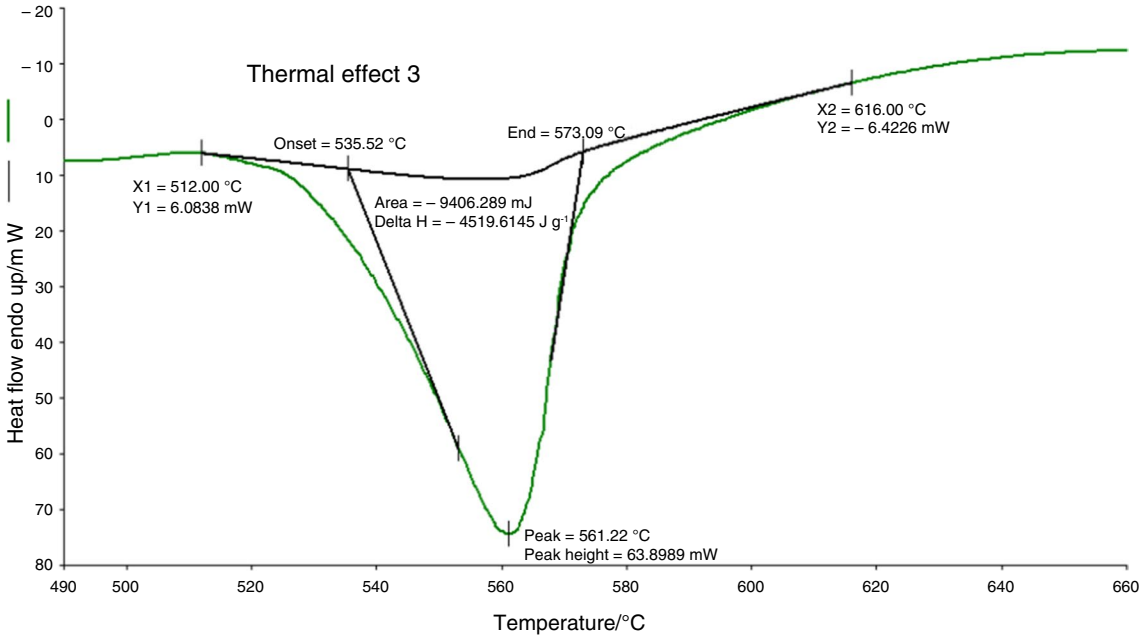

Fig. 13 Thermal effect 3 of the decomposition of Sunset Yellow in air atmosphere with 10 °C min^{-1}

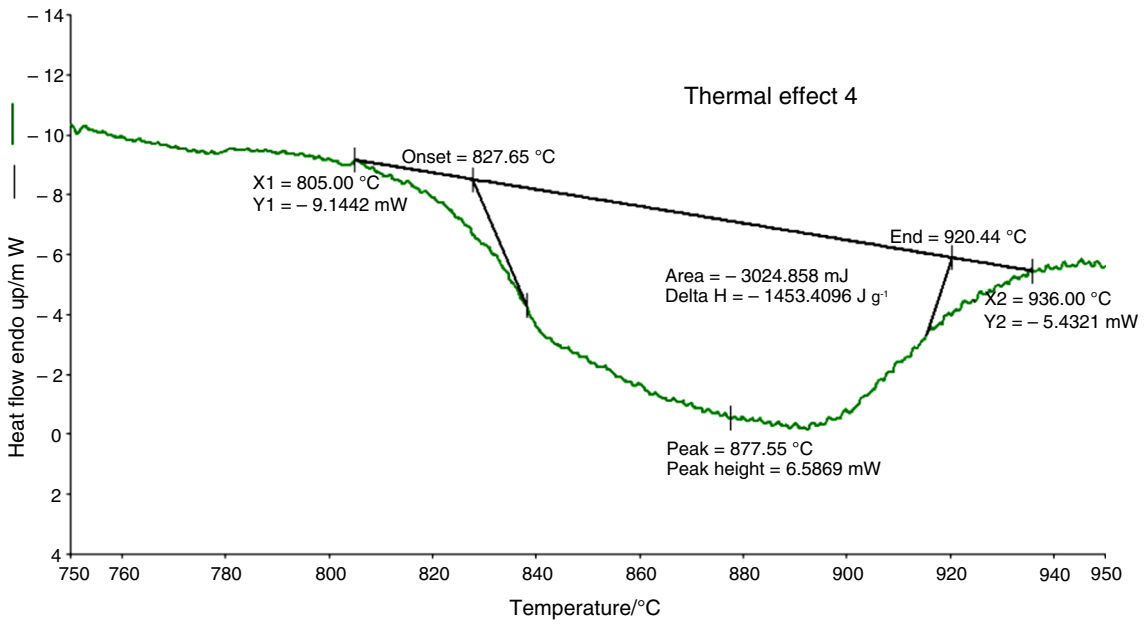

Fig. 14 Thermal effect 4 of the decomposition of Sunset Yellow in air atmosphere with 10 °C min^{-1}

Folin–Ciocâlteu (FC) reagent reacts with the reducing substance (antioxidant) in an alkaline medium (sodium carbonate), with the formation of chromogens (oxides of blue tungsten—W_8O_{23} and molybdenum—Mo_8O_{23}), which can be detected by spectrophotometry at 660 nm or 750 nm [81–84].

The antioxidant activity of Sunset Yellow is shown in Table 12:

The GAE values in the table indicate the antioxidant activity of Sunset Yellow at the three concentrations. Sunset Yellow has *antioxidant activity* at all three concentrations,

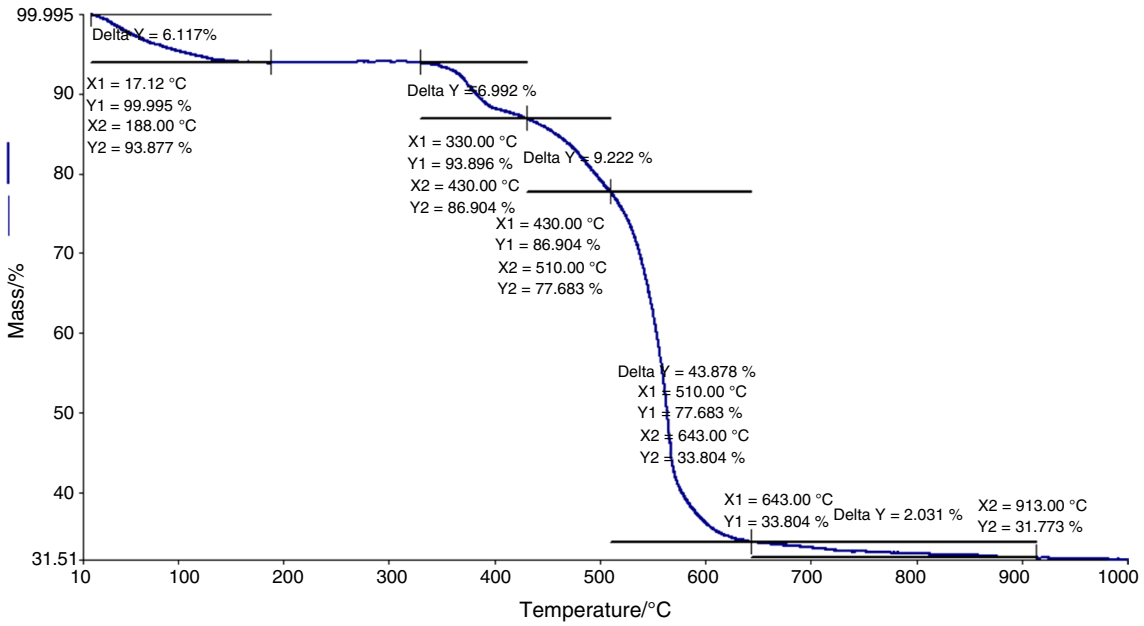

Fig. 15 Thermogravimetric details of the behaviour Sunset Yellow when decomposing in the air atmosphere, with 10 °C min^{-1}

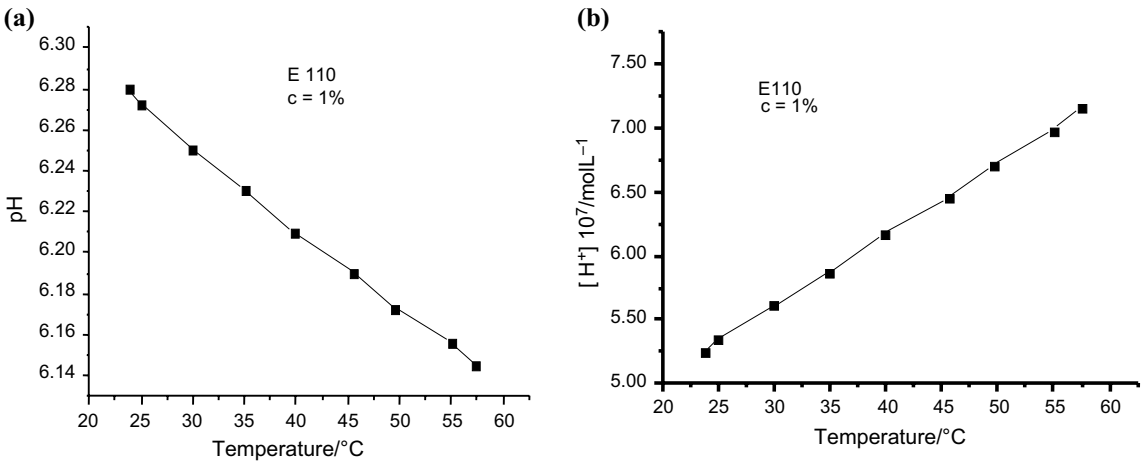

Fig. 16 **a** PH variation with temperature and **b** proton concentration [H.$^{+}$] in the aqueous solution of $c = 1\%$ Sunset Yellow (E110)

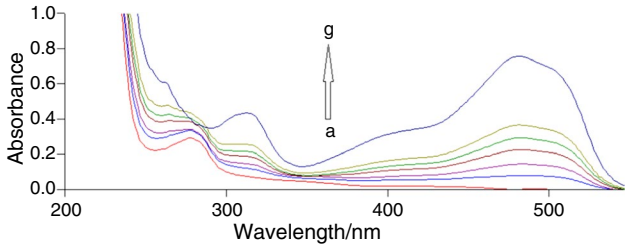

Fig. 17 Absorption spectrum of Sunset Yellow-BSA system at pH = 7.4, $c_{BSA} = 5 \times 10^{-6}$ M and $c_{\text{Sunset Yellow}} = 0$, 1, 2, 3, 4 and 5×10^{-5} M (**b** → **g**), curve **a** corresponds to the UV–Vis spectrum of BSA at $c_{BSA} = 5 \times 10^{-6}$ M, and curve **g** corresponds to the UV–Vis spectrum of Sunset Yellow, $c_{\text{Sunset Yellow}} = 5 \times 10^{-5}$ M

the highest value being at the concentration $c = 0.25\%$, which is probably due to the phenolic hydroxyl group.

(d) Phytotoxicity of Sunset Yellow

Sunset Yellow's phytotoxicity [87, 88] was studied using 4 samples. For each sample, five wheat grains are displayed in four Petri plates. Three samples were treated daily with 10 mL of Sunset Yellow aqueous solution with concentrations of 0.01, 0.05 and 0.25%. One of the Petri dishes contained the witness sample (W)—five wheat grains, treated daily with 10 mL of ultrapure water. The roots of the five

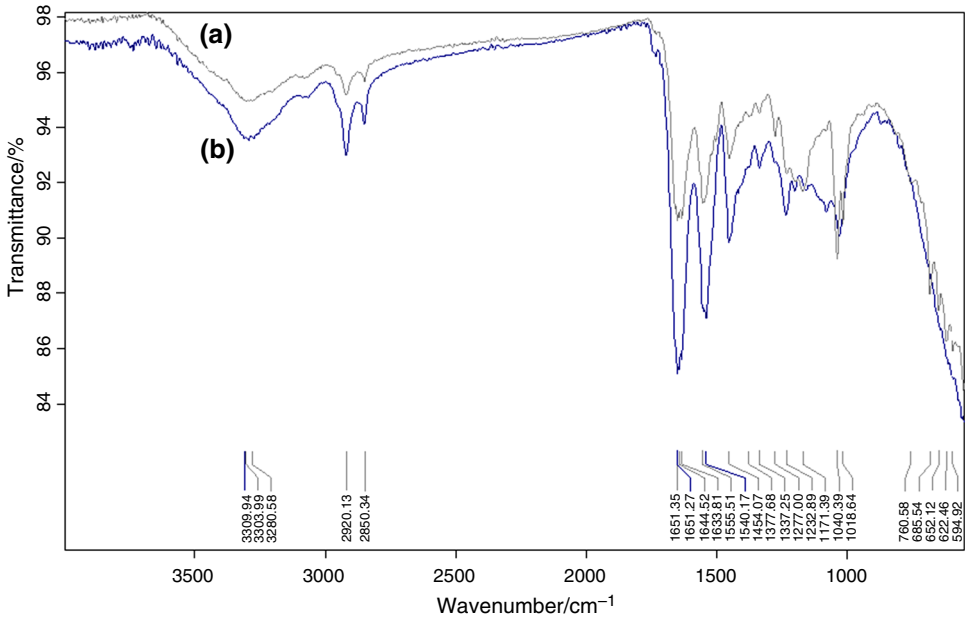

Fig. 18 FTIR spectrum of **a** treated and **b** untreated skin with Sunset Yellow solution ($c = 5\%$)

Table 12 Antioxidant activity of Sunset Yellow (E110) solution of different concentrations [85, 86]

Sample solution of Sunset Yellow (E110)	Absorbance	GAE/mg·L^{-1}
E110 ($c = 0.01\%$) + FC	0.138	3.463
E110 ($c = 0.05\%$) + FC	0.485	88.097
E110 ($c = 0.25\%$) + FC	2.002	458.097

Table 13 Average length of the roots, depending on the growth time and concentration of the Sunset Yellow's solutions

Time/h	Average length of the roots/cm			
	Concentration of Sunset Yellow/%			
	0.00*	0.01	0.05	0.25
0	2.34	2.46	2.36	2.22
24	2.54	2.60	3.16	2.50
48	2.64	2.96	3.52	2.86
72	3.9	3.58	4.06	3.80
96	4.4	4.38	4.74	4.42

*Witness sample = 0.00% Sunset Yellow

wheat seeds in each Petri dish were measured daily [89] for 4 days and an arithmetic mean was made to find out the mean value of the roots length of sample W and the mean value of the roots length of samples treated with Sunset Yellow at the three concentrations (Table 13).

By measuring the length of the roots and observing the appearance of the wheat stalks (Triticum aestivum), in the case of wheat treated with E110 (Sunset Yellow), an additional increase was observed compared to the control sample, as seen in Fig. 19 and as shown in Table 13. A fertilization effect for wheat grains growth was observed for all three concentrations.

There was also a slight bending of the wheat strains treated with Sunset Yellow (at 0.01% and 0.05% concentrations), compared to the straight strains of the control sample W, and a discolouration of the strains (at concentrations of 0.05% and 0.25%), compared to the green stems of sample W, as shown in Fig. 19. During days three and four with of Sunset Yellow treatment, it was observed that wheat developed new, vigorous roots, probably in correlation with its intense antioxidant activity. Treating wheat with aqueous solutions of Sunset Yellow at concentrations of 0.01–0.05% could increase its resistance to drought conditions.

It can be concluded that at low concentrations, Sunset Yellow does not harm the growth of wheat, but is even a growth stimulant, but at higher concentrations (0.25%), there are slowdowns in wheat growth compared to the control sample W.

Fig. 19 The phytotoxicity experiment for samples containing Sunset Yellow aqueous solutions at three concentrations (0.01, 0.05 and 0.25%) and witness sample containing 0.00% Sunset Yellow, **a** on the first day, and **b** on the fourth day

Conclusions

As the temperature increases in the range of 15–50 °C, the values of the refractive indices of Sunset Yellow solutions are decreasing, the behaviour depending on the concentration of the dye. The acidity and electrical susceptibility of aqueous Sunset Yellow solutions also depend on concentration; therefore, the Sunset Yellow content of the food can be identified.

The FTIR, Raman, UV–Vis and THz spectroscopic analyses have determined the radiation absorption lines and bands based on which the atoms, groups of atoms and the bonds responsible for these absorptions were identified. The THz absorption spectrum of Sunset Yellow obtained in the frequency range 0.2–4.5 THz allows the identification of the presence of the dye in any food using the specific absorption frequencies of Sunset Yellow which constitutes the THz spectral signature of the dye (0.76, 1.61, 1.67, 1.74, 1.80, 2.01, 2.65 and 3.54 Tz).

By laser irradiation with wavelength 476.5 nm, fluorescence of the Sunset Yellow was produced, establishing the transitions at the electron de-excitation of all elements. The laser fluorescence spectral lines may belong to the fluorescence of two or more chemical elements, which explains the high intensity of certain spectral lines of fluorescence, but there are also fluorescence spectral lines that are emitted by a single element.

Sunset Yellow is a crystalline substance at room temperature, with crystallites between 5 and 20 µm. Thermal analysis and calorimetry study performed in air indicate the evaporation of adsorbed water up to 188 °C, after which the material is thermally stable up to 330 °C. Oxidative decomposition takes place in four exothermic stages, of which the main one is between 510 and 643 °C with heat release of 4519.6 J g^{-1}. At 913 °C, the residue of 31.77% is obtained. Sunset Yellow, used for colouring processed foods, can be safely used at temperatures below 330 °C (it is recommended that foods containing this azo dye be thermally processed in an oxygen-poor atmosphere—preferably in closed containers.

Sunset Yellow bioactivity was highlighted by its interaction with proteins (collagen and bovine serum albumin—BSA), by its antioxidant activity and its phytotoxicity on wheat. The results indicated that as the concentration of Sunset Yellow in the solution increases, BSA can bind the food dye azo forming a complex with the dye. This can disrupt the normal biological function of BSA. Sunset Yellow has an undesirable effect on collagen and poses a potential risk to the skin. The antioxidant activity of Sunset Yellow increases with increasing its concentration, the highest value of GAE equivalent gallic acid (458.1 mg L^{-1}), being recorded for the concentration of 0.25%, most likely due to the presence of hydroxyl group. Treating wheat with aqueous Sunset Yellow solutions, at concentrations of 0.01–0.05%, could increase its resistance to drought conditions. At low concentrations, Sunset Yellow does not harm wheat, but at concentrations above 0.25%, there are negative changes in wheat growth.

References

1. EFSA Panel on Food Additives and Nutrient Sources added to Food (ANS). Scientific opinion on the re-evaluation of Sunset Yellow FCF (E 110) as a food additive on request from the European Commission. EFSA J. 2009;7:1330.
2. EFSA Panel on Food Additives and Nutrient Sources added to Food (ANS). Reconsideration of the temporary ADI and refined exposure assessment for Sunset Yellow FCF (E 110). EFSA J. 2014;12:3765.
3. König J. Food colour additives of synthetic origin, in Colour Additives for Foods and Beverages. Woodhead Publishing Cambridge; 2015.

4. Codex Alimentarius Commission. Class Names and the International Numbering System for food additives CAC/GL 36–1989. Codex Alimentarius FAO/WHO; 2018.
5. Compendium of food additive specifications. Food and Agriculture Organization and World Health Organization. Rome; 2016.
6. Regulation (EU) No 1129/2011 of 11 November 2011 amending Annex II to Regulation (EC) No 1333/2008 of the European Parliament and of the Council by establishing a Union list of food additives. OJ L 295; 2011.
7. https://pubchem.ncbi.nlm.nih.gov/compound/Sunset Yellow. Accessed at 28 June 2019.
8. Vlase L, Muntean D, Cobzac SC, Filip L. Development and validation of an HPLC-UV method for determination of synthetic food colorants. Rev Roum Chim. 2014;59:719–25.
9. Pagacikova D, Lehotay J. Determination of synthetic colors in meat products using high-performance liquid chromatography with photodiode array detector. J Liq Chromatogr Relat Technol. 2015;38:579–83.
10. Rovina K, Acung LA, Siddiquee S, et al. Extraction and analytical methods for determination of Sunset Yellow (E110)—a review. Food Anal Methods. 2017;10:773–87.
11. Vlase T, Vlase G, Modra D, Doca N. Thermal behaviour of some industrial and food dyes. J Therm Anal Calorim. 2007;88:389–93.
12. Constantinescu C, Morintale E, Emandi A, Dinescu M, Rotaru P. Thermal and microstructural analysis of Cu(II) 2,20-dihydroxy azobenzene and thin films deposition by MAPLE technique. J Therm Anal Calorim. 2011;104:707–16.
13. Moanta A, Ionescu C, Rotaru P, Socaciu M, Harabor A. Structural characterization, thermal investigation, and liquid crystalline behavior of 4-[(4-chlorobenzyl) oxy]-3, 4′-dichloroazobenzene. J Therm Anal Calorim. 2010;102:1079–86.
14. Gur M, Kocaokutgen H, Tas M. Synthesis, spectral, and thermal characterisations of some azo-ester derivatives containing a 4-acryloyloxy group. Dyes Pigments. 2007;72:101–8.
15. Rotaru A, Brătulescu G, Rotaru P. Thermal analysis of azoic dyes; Part I. Non-isothermal decomposition kinetics of [4-(4-chlorobenzyloxy)-3-methylphenyl](*p*-tolyl)diazene in dynamic air atmosphere. Thermochim Acta. 2009;489:63–9.
16. Moanta A, Ionescu C, Dragoi M, Tutunaru B, Rotaru P. A new azo-ester: 4-(phenyldiazenyl)phenyl benzene sulfonate—spectral, thermal, and electrochemical behavior and its antimicrobial activity. J Therm Anal Calorim. 2015;120:1151–61.
17. Moanta A, Samide A, Rotaru P, Ionescu C, Tutunaru B. Synthesis and characterization of novel furoate azodye using spectral and thermal methods of analysis. J Therm Anal Calorim. 2015;119:1039–45.
18. Rotaru A, Jurca B, Moanta A, Salageanu I, Segal E. Kinetic study of the thermal decomposition of some aromatic ortho-chlorinated azomonoethers. 1 Decomposition of 4-[(2-chlorobenzyl)oxi]-4′-triflouromethyl-azobenzene. Rev Roum Chim. 2006;51:373–8.
19. Rotaru A, Dumitru M. Thermal behaviour of CODA azoic dye liquid crystal and nanostructuring by drop cast and spin coating techniques. J Therm Anal Calorim. 2017;127:21–32.
20. Rotaru A, Constantinescu C, Rotaru P, Moanţă A, Dumitru M, Socaciu M, Dinescu M, Segal E. Thermal analysis and thin films deposition by matrix assisted pulsed laser evaporation of a 4CN type azomonoether. J Therm Anal Calorim. 2008;92:279–84.
21. Rotaru A, Moanta A, Constantinescu C, Dumitru M, Manolea HO, Andrei A, Dinescu M. Thermokinetic study of CODA azoic liquid crystal and thin films deposition by matrix-assisted pulsed laser evaporation. J Therm Anal Calorim. 2017;128:89–105.
22. Sela SK, Nayab-Ul-Hossain AKM, Hasan N, Zubair Hussain S, Sadam S. Surface modification and qualitative natural coloring of raw jute to reduce electrical resistance and induce antimicrobial properties. Appl Surf Sci Adv. 2020;1:100018.
23. Rotaru A, Moanta A, Popa G, Rotaru P, Segal E. Thermal decomposition kinetics of some aromatic azomonoethers. Part IV. Non-isothermal kinetics of 2-allyl-4-((4-(4-methylbenzyloxy) phenyl) diazenyl)phenol in air flow. J Therm Anal Calorim. 2009;97:485–91.
24. Rotaru A, Moanta A, Rotaru P, Segal E. Thermal decomposition kinetics of some aromatic azomonoethers. Part III. Non-isothermal study of 4-[(4-chlorobenzyl)oxy]-4′-chloroazobenzene in dynamic air atmosphere. J Therm Anal Calorim. 2009;95:161–6.
25. Rotaru A, Kropidlowska A, Moanta A, Rotaru P, Segal E. Thermal decomposition kinetics of some aromatic azomonoethers. Part II. Non-isothermal study of three liquid crystals in dynamic air atmosphere. J Therm Anal Calorim. 2008;92:233–8.
26. Leulescu M, Iacobescu G, Bojan M, Rotaru P. Ponceau 4R azoic red dye. Thermal behavior, optical anisotropy and terahertz spectroscopy study. J Therm Anal Calorim. 2019;138:2091–101.
27. Rotaru A, Gosa M, Segal E. Isoconversional linear integral kinetics of the non-isothermal evaporation of 4-[(4-chlorobenzyl)oxy]-4′-trifluoromethyl-azobenzene. Stud Univ Babes-Bolyai Chem. 2011;54:185–92.
28. Rotaru A. Discriminating within the kinetic models for heterogeneous processes of materials by employing a combined procedure under TKS-SP 2.0 software. J Therm Anal Calorim. 2016;126:919–32.
29. Kucerik J, David J, Weiter M, Vala M, Vynuchal J, Ouzzane I, Salyk O. Stability and physical structure test of piperidyl and morpholinyl derivatives of diphenyl-diketo-pyrrolopyrroles (DPP). J Therm Anal Calorim. 2012;108:467–73.
30. Qiu J, Tang B, Ju B, Xu Y, Zhang S. Stable diazonium salts of weakly basic amines—Convenient reagents for synthesis of disperse azo dyes. Dyes Pigments. 2017;136:63–9.
31. Moanta A. Organic chemistry and pollution. Craiova: SITECH House; 2009. p. 78–86.
32. Suzuki Y, Horie M, Okamoto Y, Kurose Y, Maeda S. Thermal and optical properties of metal azo dyes for digital video disc-recordable discs. Jpn J Appl Phys. 1998;37:2084–8.
33. El-Sonbati AZ, Diab MA, El-Bindary AA, Shoair AF, Hussein MA, El-Boz RA. Spectroscopic, thermal, catalytic and biological studies of Cu(II) azo dye complexes. J Mol Struct. 2017;1141:186–203.
34. Leulescu M, Rotaru A, Moanţă A, Iacobescu G, Pălarie I, Cioateră N, Popescu M, Criveanu MC, Morîntale E, Bojan M, Rotaru P. Azorubine: physical, thermal and bioactive properties of the widely employed food, pharmaceutical and cosmetic red azo dye material. J Therm Anal Calorim. 2021;143:3945–67.
35. Fioru L, Langfeld HW, Tarabasanu-Mihaila C. Azo dyes. Technical Publishing House; 1981.
36. Kazem-Rostami M. Factors influencing the thermal stability of azo and bisazo compounds. J Therm Anal Calorim. 2020;140:613–23.
37. Jianu D, Soare B, Matei L. Microscopic optical properties of transparent minerals in polarized light. old.unibuc.ro. 2007. Accessed at June 2018.
38. https://www.microscopyu.com/techniques/polarized-light/principles-of-birefringence. Accessed at Oct 2018.
39. Pălărie I. Spectroscopy. Practical work. University of Craiova Publishing House; 2004.
40. Palarie I, Varut MC, Chirigiu LME. Method of determination of rivanol by laser induced fluoroscence. Rev Chim Buchar. 2019;70:140–2.
41. Bojan M, Damian V, Fleaca C, Vasile T. Terahertz spectroscopic investigations of hazardous substances. Proc SPIE Proc Ser. 2016;10010:6.
42. Leulescu M, Rotaru A, Pălarie I, Moanţă A, Cioateră N, Popescu M, Morîntale E, Bubulică MV, Florian G, Hărăbor A, Rotaru P.

Tartrazine: physical, thermal and biophysical properties of the most widely employed synthetic yellow food—colouring azo dye. J Therm Anal Calorim. 2018;134:209–31.
43. Leulescu M, Pălarie I, Moanţă A, Cioateră N, Popescu M, Morîntale E, Văruţ MC, Rotaru P. Brown HT: physical, thermal and biophysical properties of the food azo dye. J Therm Anal Calorim. 2019;136:1249–68.
44. Peica N. Vibrational spectroscopy and density functional theory calculations on biological molecules. Dissertation. Würzburg; 2006.
45. Socrates G. Infrared and Raman characteristic group frequencies: tables and charts. 3rd ed. Chichester: Wiley; 2004.
46. http://www.spectroscopictools-science-and-funde/tools/. Accessed at 24 Oct 2017.
47. Atkins PW, de Paula J. Physical chemistry for the life sciences. New York: W. H. Freeman and Company; 2006.
48. Silverstein RM, Webster FX, Kiemle DJ. Spectrometric identification of organic compounds. New York: Wiley; 2005.
49. https://pubchem.ncbi.nlm.nih.gov/compound/Sodium-1-naphthalenesulfonate#section=FTIR-Spectra. Accessed at 19 Apr 2019.
50. https://pubchem.ncbi.nlm.nih.gov/compound/Sunset-Yellow-FCF#section=Spectral-Information. Accessed at 28 June 2019.
51. https://www.nist.gov/pml/atomic-spectra-database. Accessed at 17 Apr 2019.
52. https://physics.nist.gov/PhysRefData/ASD/lines_form.html. Accessed at 17 Apr 2019.
53. Shen YC. Terahertz pulsed spectroscopy and imaging for pharmaceutical applications: a review. Int J Pharm. 2017;417:48–60.
54. Zhong S, Shen YC, Ho L, Mayd RK, Zeitler JA, Evans M, Taday PF, Pepper M, Rades T, Gordon KC, Müller R, Kleinebudde P. Non-destructive quantification of pharmaceutical tablet coatings using terahertz pulsed imaging and optical coherence tomography. Opt Lasers Eng. 2011;49:361–5.
55. Lin H, Dong Y, Shen Y, Zeitler JA. Quantifying pharmaceutical film coating with optical coherence tomography and terahertz pulsed imaging: an evaluation. Wiley Online Library; 2015.
56. Zeitler JA, Shen Y, Baker C, Taday PF, Pepper M, Rades T. Analysis of coating structures and interfaces in solid oral dosage forms by three dimensional Terahertz Pulsed Imaging. Wiley InterScience; 2006.
57. Gowen AA, O'Sullivan C, O'Donnell CP. Terahertz time domain spectroscopy and imaging: emerging techniques for food process monitoring and quality control. Trends Food Sci Technol. 2012;25:40–6.
58. Parrott EPJ, Sun Y, Pickwell-MacPherson E. Terahertz spectroscopy: its future role in medical diagnoses. J Mol Struct. 2011;1006:66–76.
59. Shen J, Wang G, Jiang D, Liang L, Xu X. Terahertz spectroscopic investigations of caffeine and 3-acetylmorphine. Int J Light Electron Opt. 2010;121:1712–6.
60. Nishikiori R, Yamaguchi M, Takano K, Enatsu T, Tani M, de Silva UC, Kawashita N, Taragi T, Morimoto S, Hangyo M, Kawase M. Application of partial least square on quantitative analysis of l-, d-, and dl-tartaric acid by terahertz absorption spectra. Chem Pharm Bull. 2008;56:305–7.
61. Segal E, Fătu D. Introduction to nonisothermal kinetics. Bucharest: Academy Publishing House; 1983.
62. Brown ME. Introduction to thermal analysis. Techniques and applications. New York: Kluwer Academic Publishers; 2004.
63. Brown ME. Handbook of thermal analysis and calorimetry, vol. 1. New York: Elsevier Science; 1998.
64. Rotaru P. Thermal properties and thermal processes of materials. Craiova: SITECH Publishing House; 2010.
65. Rotaru A, Moanta A, Salageanu I, Budrugeac P, Segal E. Thermal decomposition kinetics of some aromatic azomonoethers. Part I. Decomposition of 4-[(4-chlorobenzyl)oxy]-40-nitroazobenzene. J Therm Anal Calorim. 2007;87:395–400.
66. Ion I, Ion A. Analytical chemistry. Chemical equilibria. Bucharest: Printech Publishing House; 1999.
67. Bhusan Jena B, Satish L, Sekhara Mahanta C, Ranjan Swain B, Sahoo H, Dash BP, Satapathy R. Interaction of carborane-appended trimer with bovine serum albumin: a spectroscopic investigation. Inorg Chim Acta. 2019;491:52–8.
68. Wen MG, Zhang XB, Tian JN, Ni SH, Bian HD, Huang YL, Liang H. Binding interaction of xanthoxylin with bovine serum albumin. J Solut Chem. 2009;38:391–401.
69. https://toxnet.nlm.nih.gov/. Accessed at 19 Apr 2019
70. Pellegrini D, Corsi M, Bonanni M, Bianchini R, D'Ulivo A, Bramanti E. Study of the interaction between collagen and naturalized and commercial dyes by Fourier transform infrared spectroscopy and thermogravimetric analysis. Dye Pigments. 2015;116:65–73.
71. Ahlstrom LH, Sparr Eskilsson C, Bjorklund E. Determination of banned azo dyes in consumer goods. Trends Anal Chem. 2005;24:49–56.
72. Golka K, Kopps S, Myslak ZW. Carcinogenicity of azo colorants: influence of solubility and bioavailability. Toxicol Lett. 2004;151:203–10.
73. Puntener A, Page C. European Ban on certain azo dyes. Qual Environ. 2004; 1–3. http://www.dyediet.com/wp-content/uploads/2012/01/European-Ban-on-certain-Azo-Dyes.pdf
74. Fragoso CT, Battisti R, Miranda C, de Jesus PC. Kinetic of the degradation of CI Food Yellow 3 and CI Food Yellow 4 azo dyes by the oxidation with hydrogen peroxide. J Mol Catal A Chem. 2009;301:93–7.
75. Parisi F. Adsorption and separation of crystal violet, Cerium(III) and Lead(II) by means of a multi-step strategy based on K10-montmorillonite. Minerals. 2020;10:466.
76. Parisi F, Lazzara G, Merli M, Milioto S, Princivalle F, Sciascia L. Simultaneous removal and recovery of metal ions and dyes from wastewater through montmorillonite clay mineral. Nanomaterials. 2019;9:1699.
77. Mallikarjuna NM, Keshavayya J, Maliyappa MR, Shoukat Ali RA, Venkatesh T. Synthesis, characterization, thermal and biological evaluation of Cu(II), Co(II) and Ni(II) complexes of azo dye ligand containing sulfamethaxazole moiety. J Mol Struct. 2018;1165:28–36.
78. Samide A, Tutunaru B, Moanţă A, Ionescu C, Tigae C, Vladu AC. A Study of the surface protective layer formedon carbon steel in water-dioxane solution containing 0.15 M NaCl in presence of an azo dye with antimicrobial activity. Int J Electrochem Sci. 2015;10:4637–53.
79. Tutunaru B, Tigae C, Spînu C, Prunaru I. Spectrophotometry and electrochemistry of Brilliant Blue FCF in aqueous solution of NaX. Int J Electrochem Sci. 2017;12:396–412.
80. Carabet CA, Moanta A, Palarie I, Iacobescu G, Rotaru A, Leulescu M, Popescu M, Rotaru P. Physical, thermal and biological properties of yellow dyes with two azodiphenylether groups of anthracene. Molecules. 2020;25:5757.
81. Folin O, Ciocalteu V. On tyrosine and tryptophane determinations in proteins. J Biol Chem. 1927;73:627.
82. Singelton VR, Orthifer R, Lamuela-Raventos RM. Analysis of total phenols and other oxidation substrates and antioxidants by means of Folin-Ciocalteu reagent. Method Enzymol. 1999;299:152–78.
83. Wojdyłoa A, Oszmiańskia J, Czemerysb R. Antioxidant activity and phenolic compounds in 32 selected herbs. Food Chem. 2007;105:940–9.

84. Büyüktuncel E, Porgali E, Çolak C. Comparison of total phenolic content and total antioxidant activity in local red wines determined by spectrophotometric methods. Food Nutr Sci. 2014;5:1660–7.
85. Frankel E, Meyer A. The problems of using one-dimensional methods to evaluate multifunctional food and biological antioxidants. J Sci Food Agric. 2000;80:1925–41.
86. Huang D, Ou B, Prior R. The chemistry behind antioxidant capacity assays. J Agric Food Chem. 2005;53:1841–56.
87. https://www.sciencedirect.com/topics/agricultural-and-biological-sciences/phytotoxicity. Accessed at 03 July 2019.
88. https://en.wikipedia.org/wiki/Phytotoxicity. Accessed at 03 July 2019.
89. https://www.iso.org/standard/51388.html. Accessed at 03 July 2019.